J. Fluid Mech. (1997), *vol.* 342, *pp.* 53–86. Printed in the United Kingdom

Structures in stratified plane mixing layers and the effects of cross-shear

By P. ATSAVAPRANEE AND M. GHARIB

Graduate Aeronautical Laboratories, California Institute of Technology, Pasadena, CA 91125, USA

(Received 20 September 1995 and in revised form 2 January 1997)

A two-dimensional temporal mixing layer is generated in a stratified tilting tank similar to that used by Thorpe (1968). Extensive flow dynamics visualization is carried out using, for the top and bottom layers, fluids of different densities but of the same index of refraction. The two-dimensional density field is measured with the laser-induced fluorescence technique (LIF). The study examines further the classical problem of the two-dimensional mixing layer and explores the effects of cross-shear on a nominally two-dimensional mixing layer, a situation widespread in complex industrial and natural flows. Cross-shear is another component of shear, in plane with but perpendicular to the main shear of the base flow, generated by tilting the tank around a second axis.

In the two-dimensional mixing layer, the pairing process is found not only to govern the growth of the mixing layer as is commonly known, but also to play a critical role in the mixing transition. The flow region between pairing vortices exhibits a complex topography of stretches and folds in the fluid interface, the length of which is measured to grow exponentially in time. But as higher stratification increasingly inhibits the pairing process, the flow topography becomes less complex, with the material interface growing less rapidly (linearly). Also, the total yield of mixed fluid, as calculated from the measurements of the density field, is reduced with higher stratification. The reduced mixing is due in part to the reduction in the fluid entrainment into Kelvin–Helmholtz vortices (both in the overall volume and in the portion of the bottom fluid to the overall volume), the reduced frequency of pairing of those vortices, and the subsequent arrest of turbulence during flow restratification. The stratified mixing layer also exhibits many interesting secondary features which have been previously documented to various degrees – the baroclinic shear-induced instability in the braid region, gravitational convective instability within the cores, vortex tearing, and vortex dislocations of the Kelvin–Helmholtz vortices.

The introduction of a critical level of cross-shear to a plane shear layer results in a new type of 'co-rotating' streamwise vortices in the braid region of the primary Kelvin–Helmholtz instability and an appreciable gain in the total yield of mixed fluid. The appearance and dynamics of the secondary streamwise vortices are very similar to those of the primary Kelvin–Helmholtz vortices, both qualitatively (dynamics of roll-up and pairing) and quantitatively (normalized length and time scales). It is also found that if cross-shear is introduced to the shear layer while it is still planar, the resulting flow behaves simply as a normal but oblique two-dimensional mixing layer. The co-rotating streamwise vortices and the corresponding added mixing result only when cross-shear is introduced after the primary shear layer has started to roll up. There is also evidence that even in the absence of 'global' cross-shear, the co-rotating streamwise vortices can develop locally where a high curvature of the density interface baroclinically induces strong local cross-shear.

1. Introduction

The physics of a free plane mixing layer is of considerable interest from both fundamental and practical points of view. It has been widely suggested that mixing in the oceans and the atmosphere is partly governed by the turbulence generated by shear-induced instabilities of the Kelvin–Helmholtz type (Woods 1968; Browning & Watkins 1970). In engineering flows, mixing layers govern, for example, the aerodynamics of vehicles, the mixing rate in chemical lasers and combustion chambers, and the spread of pollutants at industrial sites. Since the two-dimensional mixing layer is very generic, with its major features shared by other turbulent shear flows, the understanding of its physics is also of interest to other shear flow problems such as jets and wakes.

Studies of plane mixing layers date as far back as 1868 with the theoretical study by Helmholtz on the dynamical instability in a homogeneous shear flow with a step discontinuity in velocity. Kelvin later extended the work to shear flows with layers of different densities, hence the name Kelvin–Helmholtz instabilities. But not until the middle of this century was significant impetus in the field revived by the detailed measurements of the state of the turbulent homogeneous mixing layer by Liepmann & Laufer (1947). Since then various studies of flow dynamics, for low-Reynolds-number (Winant & Browand 1974), high-Reynolds-number (Brown & Roshko 1974; Dimotakis & Brown 1976; Koochesfahani & Dimotakis 1986), and stratified (Koop & Browand 1979) flows, have revolutionized our physical understanding by clearly demonstrating the roles of coherent large-scale vortical structures in the overall dynamics, the turbulent transition (the onset of random three-dimensional small-scale motions), and the turbulent transport processes.

Relatively recently, three-dimensional coherent structures in a plane mixing layer have been studied in some detail with the recognition that they could have a crucial role in the turbulent processes. Konrad (1977) and Breidenthal (1978) found that the mixing transition is preceded by the appearance of spanwise sinuous disturbances of the Kelvin–Helmholtz vortices, downstream of which streamwise streaks are observed. Bernal & Roshko (1986) later determined that these streaks are streamwise counter-rotating vortices that are superimposed upon the primary spanwise vortex structures, and that they contribute not only to mixing of passive scalars but also to all components of the Reynolds stress. The flow visualization by Lasheras & Choi (1988) in a low-Reynolds-number shear layer with a sinusoidal spanwise forcing clearly provides strong supporting evidence of the earlier interpretations of the dynamics of the counter-rotating streamwise vortices.

Previous research has also identified other possible mechanisms by which small-scale velocity fluctuations are generated in a turbulent mixing layer. In a stratified mixing layer, a gravitational instability in the statically unstable regions of the Kelvin–Helmholtz vortices has been identified as an important mixing mechanism (Thorpe 1971, 1985; Klassen & Peltier 1985; Schowalter, Van Atta & Lasheras 1994). Browand & Troutt (1980) observed that in a high-Reynolds-number turbulent mixing layer local interactions between adjacent vortices can result in 'branching' or 'dislocation' of the vortex structures where one vortex can partly merge with another to form a tree-branch type pattern. The process of vortex tearing, in which a smaller Kelvin–Helmholtz structure is caught within the strain field between two larger vortices, has also been routinely predicted by many researchers. Other secondary instabilities, such as the baroclinically generated shear-induced instability in the braid region (Thorpe 1971, 1987; Staquet 1995) and three-dimensional tubes and knots (Thorpe 1987), also contribute to the transport processes in a turbulent stratified mixing layer.

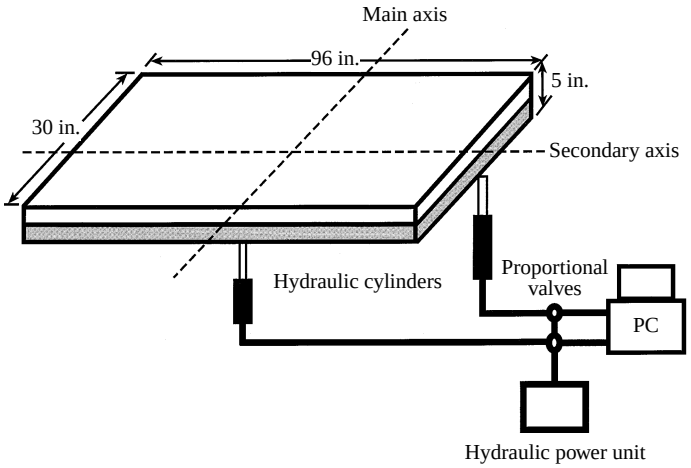

FIGURE 1. Tank schematic (not to scale).

The main fundamental objectives of the current work are to gain better understanding of the turbulent processes in a stratified mixing layer and to explore a complex flow scenario that has thus far not been studied. A scenario likely to be encountered in a complex industrial or natural shear flow would be that while a two-dimensional shear layer is developing, the base flow could easily shift in an oblique direction (in the original plane), effectively adding another component of shear (cross-shear) to the shear layer. Some specific questions that we hope to answer are:

What are the roles of the different processes and instabilities involved in the turbulent transition in the plane mixing layer?

What effects does stratification have on the large-scale dynamics and the small-scale scalar mixing in the mixing layer?

What are the effects on the mixing layer when cross-shear is introduced? Does the presence of cross-shear alter the main features of the mixing layer or introduce any new instability?

2. Experimental apparatus and methods

2.1. *The tilting tank*

The experiment is performed in an apparatus similar to that used by Thorpe (1968) and in his subsequent work. The schematic of the set-up is illustrated in figure 1. An enclosed tank, 2.44 m long $\times$ 0.762 m wide $\times$ 12.7 cm deep is filled through four 1.3 cm diameter openings on the bottom of the tank, first halfway with either fresh water or ethanol–water solution, and then slowly with epsom-salt–water solution until full. In order to obtain a sharp interface, mixing between the two layers during the filling process is kept to a minimum with the use of a horizontal deflector plate placed slightly above the fill holes. At the interface a density-gradient layer is formed whose thickness can be controlled by allowing the layer the appropriate time to grow with diffusion. The density difference between the two layers is varied between 0.005 and 0.08 g cm^{-3}, and the bottom layer takes about 1 hour to fill. The thickness of the density interface can be made as sharp as 4 mm, giving a spanwise aspect ratio of about 190. The stratified fluid is allowed to sit until the required density-layer thickness is attained and all the disturbances from the filling process have died down, before the flow is generated by tilting the tank off the initially horizontal level.

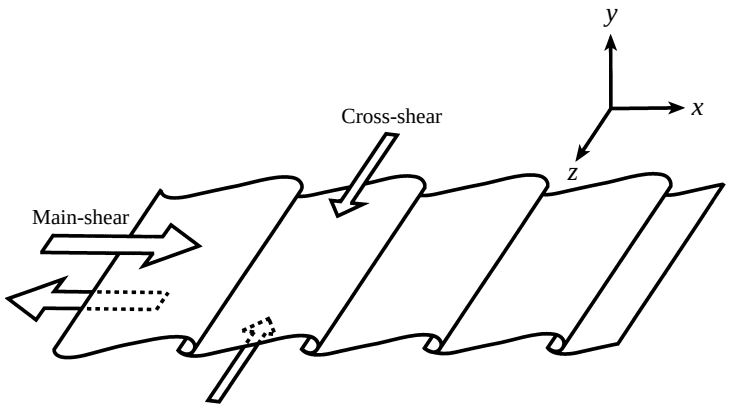

FIGURE 2. A schematic showing the overall picture of a mixing layer with cross-shear.

Tilting of the tank provides the potential for the two layers to accelerate in opposite directions, resulting in a velocity shear at the interface. A PC regulates the tilting process with control signals that provide the tank with smooth angular acceleration and deceleration in order to minimize vibrations and possible disturbances to the flow (the tank is tilted through an angle of 8–16° in about 3 s). The density stratification, density-layer thickness, tilt angle, and the time the tank is left in the tilted position are chosen carefully to obtain the desired experimental parameters (see the Appendix). A certain time t_o after the tank is tilted, it is usually tilted back to the horizontal position to create a steady flow for the development of the Kelvin–Helmholtz instability which forms at the interface. In a few cases in which the stratification is low and the time it takes for the flow to accelerate to the desired Reynolds number is long, the tank is left in the tilted position throughout the development of the flow. In these cases, a steady flow is not achieved, but the acceleration is low enough that the flow can be considered quasi-steady.

The tank is designed so that it can be tilted around two independent axes of rotation, which lie about 20 cm below the fluid interface (this gap allows flow visualization from the side, and care is taken so that it does not affect the flow development by using a low tilt speed). For the study of the classic two-dimensional mixing layer, the base flow of the shear layer is generated by tilting the tank around only the main axis and back to horizontal before Kelvin–Helmholtz roll-up. To study the effect of cross-shear on a nominally two-dimensional mixing layer, the tank is first tilted around the main axis, generating the main shear; and a moment later, with the primary shear layer still evolving, the tank is tilted around the second axis and back, for the cross-shear. A schematic of the flow is shown in figure 2. The streamwise direction is defined as the direction of the main base flow (x-axis), and the spanwise direction is along the axis of the main Kelvin–Helmholtz vortices (z-axis).

The parameter range in most of the present experiments is such that the presence of density stratification has important dynamical consequences on the development of the mixing layer. The flow is characterized by the velocity difference of the mean flow and the density difference of the two layers. The shear layer has two vertical length scales: δ_v, defined as the maximum velocity-gradient thickness $\Delta U/(\partial u/\partial y)_{max}$; and δ_ρ, the maximum density-gradient thickness $\Delta\rho/(\partial\rho/\partial y)_{max}$. Right after the flow is generated by tilting the tank δ_v is initially equal to δ_ρ (because outside the layer with density gradient, the fluid would be of uniform velocity) but grows with diffusion as the free-stream accelerates (see Appendix). It generally does not increase more than 40 %

before the initial instability appears so that $1 \leqslant \delta_v/\delta_\rho \leqslant 1.40$. The flow is uniquely determined by the following non-dimensional parameters:

$$Ri_i = g\Delta\rho\delta_v/\rho_{av}(\Delta U)^2, \quad Re_i = \Delta U\delta_v/\nu, \quad Sc = \nu/D, \quad \delta_v/\delta_\rho,$$

where ν and D are the kinematic viscosity and the molecular diffusivity of water, respectively. Ri_i and Re_i are the initial Richardson number and Reynolds number, measured at the onset of the Kelvin–Helmholtz instability (the instant the shear layer is observed to deviate from a simple parallel flow), respectively. The Reynolds number is around 2000 for most experiments, corresponding to a typical absolute velocity in each layer of 12 cm s^{-1} in opposite directions. The Richardson number ranges from 0.16 to 0.01. Sc is the Schmidt number which is fixed at about 600.

The range of experimental parameters is limited by the physical size of the apparatus. The typical thickness of the density interface is 6 mm, which depending on the Richardson number, corresponds to a maximum vertical size of 3 to 5 cm for the Kelvin–Helmholtz vortices. Large tilt angles of between 8 to 16° are used in order to minimize the top and bottom 99% boundary layer thickness which typically does not exceed 2 cm when the mixing layer is fully turbulent. The return surges from the ends of the tank limit the running time of the experiments but normally reach the middle of the tank well after the mixing layer becomes fully turbulent.

2.2. *Matching the index of refraction*

It is necessary to match the index of refraction of the two layers for flow visualization and density-field measurement purposes. As described by McDougall (1979) the use of two appropriate solutions can result in such a match while retaining the desired density stratification. McDougall found two appropriate choices of solutes: ethanol and table salt, epsom salt and sugar. In this study ethanol and epsom salt are found to form an appropriate pair of solutes, yielding very good optical results and proving stable to double-diffusive instability of the salt-fingering type when the layers are stably stratified. A typical density difference between the two layers is 0.02 g cm^{-3}, with the matched index of refraction of 1.3355. The solutions for the two layers are prepared by mixing the appropriate amount of solute with water in separate tanks such that the desired density stratification is obtained and the indices of refraction of the two solutions are the same. A hand-held refractometer with an accuracy of 0.0001 is used to measure the index of refraction. Care is also taken to ensure that the temperature of the two premixed layers, measured with a high-resolution thermometer, matches to within 0.01 °C. This step eliminates any variation in the index of refraction due to thermal distortion or any convective instability arising from unstable temperature gradients. A peristaltic pump is used to fill the tank in order to minimize heating of the fluids. A simple fluid 'capacitor' is designed and installed along the filling line so that the flow output experiences minimum pulsation from the peristaltic pump.

2.3. *Laser-induced fluorescence* (*LIF*)

Two-dimensional planes in the flow are visualized using a laser-induced fluorescent dye. Sodium fluorescein (uranine) is premixed with the fluid of the bottom layer, and its fluorescence is excited by an argon–ion laser sheet. The schematic of the flow visualization/recording system is presented in figure 3. The beam of an argon–ion laser is collimated into a thin beam and passed through a cylindrical lens to form a sheet about 0.5–1 mm thick. Special care is taken to achieve a maximum uniformity of the laser sheet fluorescence by using a very small dye concentration of 4.2×10^{-7} M (molarity) to minimize laser attenuation due to dye absorption, and long focal lengths for both the collimator lens and the cylindrical lens to minimize variations of the sheet

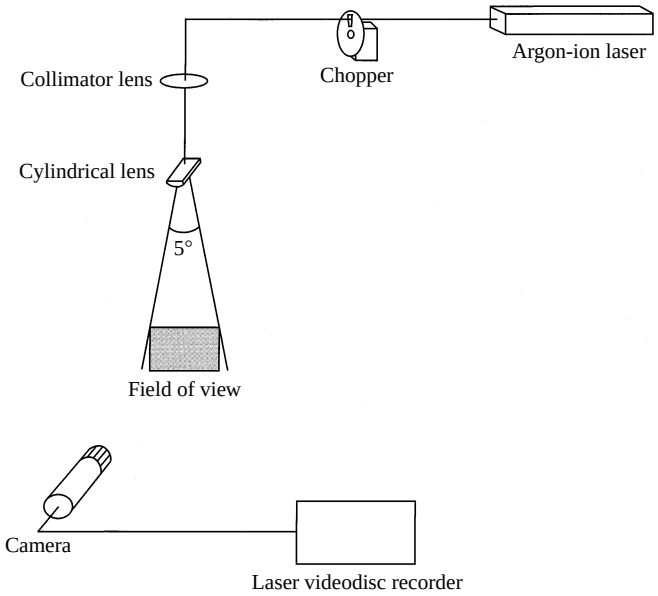

FIGURE 3. Flow visualization/recording system.

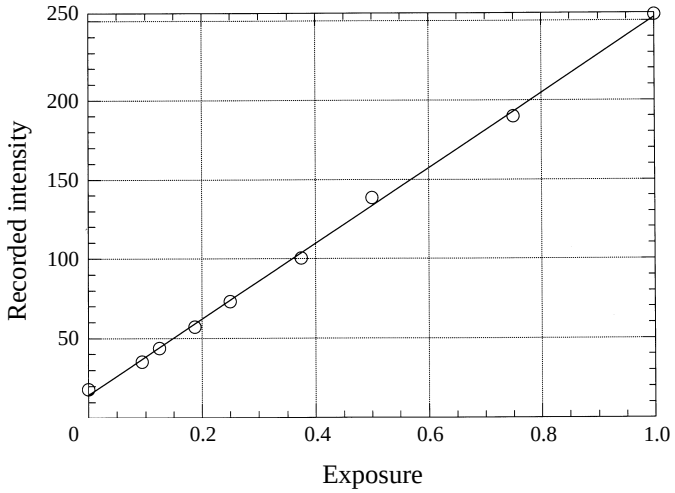

FIGURE 4. The response curve of the recording system.

intensity. Images are acquired with a Texas Instrument MC-1134GN CCD camera and recorded on a Sony laser videodisc recorder LVR-5000A at 30 frames per second. The measured response curve of the recording system, shown in figure 4, is found to be linear. The CCD array is 1134 pixels $\times$ 486 pixels, and the recorded images are digitized to 768 pixels $\times$ 480 pixels. The typical field of view of the images is 15.2 cm $\times$ 11.4 cm, yielding a spatial resolution in the object plane of about 200 μm $\times$ 240 μm. The laser beam is shuttered by a chopper with a temporal resolution (the shutter speed) of 2 ms. Note that for dynamic conditions, the actual spatial resolution can be as much as 450 μm $\times$ 300 μm because of the smearing as fluid convects past the pixels within the 2 ms exposure time.

2.4. *Plan-view visualizations*

The plan view of the mixing layer is visualized in two ways. The first method is the standard shadowgraph technique (no dye nor index of refraction matching), and the second method is similar to that used by Lasheras & Choi (1988). The interface between the two streams can be visualized by premixing the bottom layer with a high concentration of a fluorescent dye and illuminating from above with flash lamps to create an opaque interface. The concentration and light attenuation of the dye are so high that the illuminating light is not able to penetrate more than a few millimetres; therefore, the image obtained through this technique effectively visualizes the interface between the two layers, creating the appearance of a 'muddy' bottom layer.

2.5. *Density field and mixing measurements*

The two-dimensional plane LIF images obtained as described in §2.3 are used to calculate the two-dimensional density field of the mixing layer, in a way similar to the line density measurements by Koochesfahani & Dimotakis (1986). As described in §2.3, special care is taken to achieve maximum uniformity of the laser sheet and minimum laser dye attenuation. If the illuminating laser sheet is perfectly uniform in the observation plane and the laser dye attenuation is infinitesimal, the density field can be easily obtained since the recorded intensity on each pixel would be directly proportional to the fluorescence from the corresponding sampling volume with a linear recording system. In turn the fluorescence from each sampling volume is directly proportional to the fractional volume of the dyed fluid at that location. It follows then that the density field can be directly obtained from the recorded intensity field. The local volume fraction of the bottom fluid is given by

$$\xi = v_b/(v_t+v_b) = (I-I_t)/(I_b-I_t),$$

where I is the fluorescence intensity recorded from a sampling volume, I_t is the noise level recorded from a sample with no dye (top fluid), and I_b is the intensity from a sample of unmixed dyed fluid. The density of the fluid in the sampling volume is

$$\rho = \rho_t(1+\xi\Delta\rho).$$

In order to utilize the two-dimensional LIF images in the calculation of the density field, the issues of laser sheet non-uniformity and laser dye attenuation need to be addressed. The long focal lengths of the collimator lens and the cylindrical lens result in a nearly parallel laser sheet, with a maximum fan angle of only 2.5° from vertical. Therefore, the laser sheet can be roughly estimated to be a parallel laser sheet which has a horizontal Gaussian profile in intensity as given by

$$I(x, Y_o) = I_{max}(Y_o)\,[1-f(x)].$$

The measured drop-off function $f(x)$ is kept small, with a maximum less than 0.1. In the vertical direction the local laser sheet intensity in the y-direction as attenuated by the fluorescent dye is given by

$$I_{absorp}(X_o, y) = I_{no\,absorp}(X_o)\exp\left(-\epsilon_o\int_0^y C_d\,\mathrm{d}y\right)$$

where ϵ_o is the dye molar absorption coefficient, and C_d is the local molar dye concentration.

Owing to the small dye concentration used, the maximum attenuation is only about 6%. A test image is taken before each run to obtain the dye molar absorption

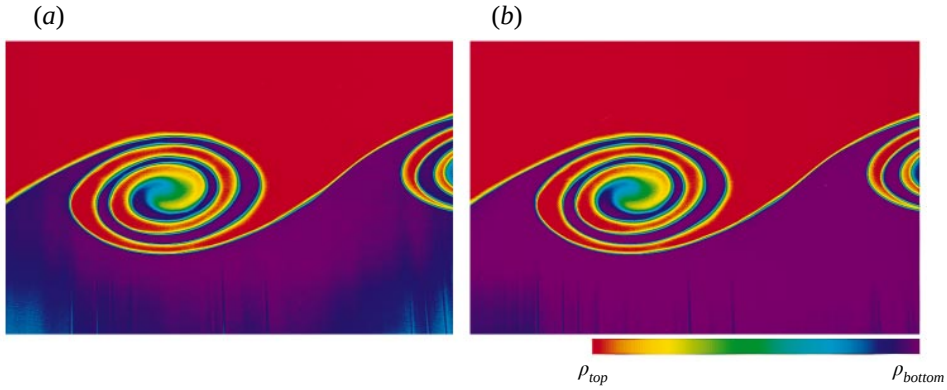

FIGURE 5. (*a*) Non-corrected image; (*b*) image corrected for horizontal Guassian laser sheet profile and laser sheet attenuation by dye absorption.

coefficient and the horizontal Gaussian profile. The intensity of each pixel is then corrected for the Gaussian profile drop-off and the laser dye attenuation as follows:

$$I_{corrected}(x,y) = I_{measured}(x,y) \Big/ \left\{ [1 - f(x)] \exp\left(-\epsilon_o \int_0^y C_a \, \mathrm{d}y \right) \right\}.$$

The method works remarkably well if the laser sheet is approximately parallel and the errors that need to be corrected are small to begin with. Figure 5(*a*) shows an example of a raw image, and figure 5(*b*) shows the corresponding corrected image, both false-colour coded for easy detection of intensity variation.

2.6. *The effect of resolution*

A fundamental problem associated with the current image recording technique is that information on the eddies of scales smaller than the spatial resolution is lost. The Batchelor scale, the smallest diffusive scale, in a two-dimensional mixing layer is estimated (Corcos & Sherman 1984) to be $\lambda_d = (\pi D/2\gamma)^{1/2}$, of the order of 20 μm under current experimental conditions, D being the molecular diffusivity and γ the maximum strain rate encountered in the flow, which is of the order of $\Delta U/\delta_\rho$. Therefore, the measurement resolution, about 450 μm × 300 μm, is severely limited and cannot resolve the smallest mixing scale when the turbulence is active. This difficulty, however, does not plague a mixing measurement made a few minutes after the mixing layer has gone through turbulent transition and relaminarization. By this time, the velocity fluctuations have died down, and all the sharp gradients have been smeared out. This measurement represents the 'total yield' of mixed fluid attained in the mixing layer and is analogous to those made by Koop & Browand (1979) in a spatial stratified mixing layer using a conductivity probe at the farthest downstream station, where the flow has relaminarized and attained its 'asymtotic' amount of mixing.

3. The two-dimensional mixing layer

3.1. *Roll-up and pairing*

A discussion of the mixing layers as observed through flow visualization is presented in this subsection and §3.2. The general characteristics of the observed Kelvin–Helmholtz instability are mainly consistent with the findings of past investigations. The flow manifests the usual dynamics: the growth of the most-amplified wavelength of the disturbances and the distortion into nonlinearity; the rolling up of the vorticity interface into Kelvin–Helmholtz vortices; the pairing of the large-scale structures;

turbulent transition; and the eventual restratification of the flow into a stable system of density layers. The density thickness of the diffusive interface is obtained before each experiment by calculating an equivalent mixed-fluid thickness δ_m, defined like a displacement thickness, from an LIF image as described in the Appendix. The density layer thickness δ_ρ is roughly twice δ_m (and would be exactly twice for a piecewise-linear density profile). The averaged δ_ρ calculated in this way is 0.60 cm and agrees well with the value measured by traversing a conductivity probe. The dimensionless wavenumber $\alpha = 2\pi/(\lambda_{KH}/\delta_\rho)$, where λ_{KH} is the wavelength of the Kelvin–Helmholtz instability, is found to be independent of the Richardson number, with an average value of 0.40 and a standard deviation of 0.05.

A few seconds after the tank is tilted, a uniform array of Kelvin–Helmholtz waves is observed. Shown in figures 6, 7 and 8 are planar cross-sections of mixing layers of similar Reynolds numbers (around 2000) and Richardson numbers of 0.012, 0.022, and 0.043, respectively. The instability waves grow with time and eventually become nonlinear, with the initially uniform vorticity layer rolling up into cat's-eye structures. At lower Richardson numbers the initial roll-up seems qualitatively unaffected by the stratification, up to the point of the maximum roller height or the 'climax' state. Note the almost symmetric nature of the Kelvin–Helmholtz vortices in figure 6. Roughly equal amounts of heavy and light fluid are entrained into the large-scale structures, as opposed to a spatial mixing layer where the faster fluid is more abundant in the cores (Koochesfahani & Dimotakis 1986).

As stratification and Richardson number increase beyond the point of validity in the Boussinesq approximation, the appearance of the large-scale Kelvin–Helmholtz vortices becomes significantly altered. Entrainment of top and bottom fluids is no longer symmetric, and a markedly reduced amount of the heavier bottom fluid is entrained into the cores. Figure 9 illustrates the appearance of the large-scale vortices at the climax state for two different Richardson numbers, 0.043 and 0.079. The ratio of the bottom fluid to the top fluid in the core varies from about 1 at $Ri = 0.012$ to 0.8 at $Ri = 0.043$ (figure 9*a*) and 0.5 at $Ri = 0.079$ (figure 9*b*). The fact that the outer band of the core material in the left-hand vortex of figure 9(*b*) cannot even complete the cat's eye further highlights the influence of moderate stratification on the dynamics of the Kelvin–Helmholtz vortices. Also the maximum vortex size attained at the climax state is reduced with higher stratification. The maximum roller height-to-wavelength ratio is measured at different Richardson numbers (for constant Reynolds number = 2000) and plotted in figure 10, along with data from Thorpe (1973). The data show that with increasing stratification, the Kelvin–Helmholtz vortices entrain less fluid into increasingly smaller cores, which are the regions most active in turbulence and mixing. Consequently the resultant amount of mixing would be reduced accordingly, as shown in the mixing measurements presented in §3.4. Beyond the Richardson number of around 0.16, the instability no longer has the appearance of a Kelvin–Helmholtz instability but rather takes the form of the Holmboe instability, in line with the findings of Koop & Browand (1979).

Beyond the climax state, the effect of stratification on the large-scale dynamics becomes evident in another manner. The average number of pairings each Kelvin–Helmholtz vortex experiences is significantly lower with increasing stratification. The vortices in the $Ri = 0.043$ case experience about 0.7 pairing each on average (the number of vortical structures involved in pairings divided by the total number of vortices), while the vortices in the $Ri = 0.012$ case experience about 1.2 pairings each. The large-scale vortices in our experiments on average experience about one fewer pairing when compared with the data by Koop & Browand (1979), whose

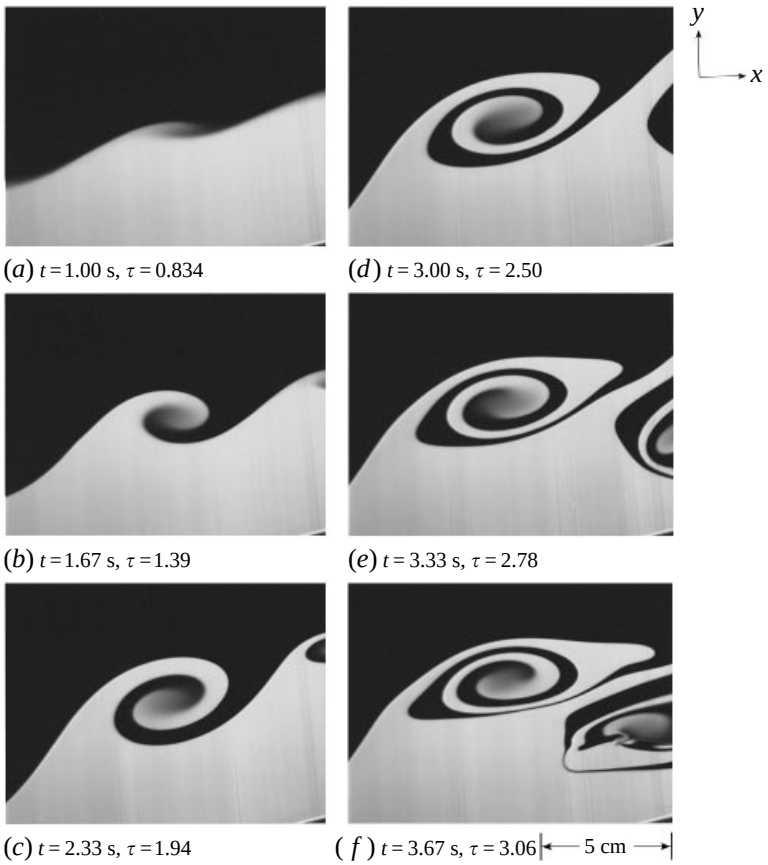

FIGURE 6 (*a–f*). For caption see facing page.

experiment was conducted at similar Richardson number but the much lower Reynolds number of 300. This discrepancy is possibly due to two effects: the higher Reynolds number in our experiments and the finite boundary effect of the tank. At a higher Reynolds number the Kelvin–Helmholtz vortices can become turbulent after fewer pairings. A vortex that has become turbulent will begin to lose the ability to mutually induce an adjacent vortex into rotation around a common centre (pairing), because some energy is lost to random small-scale motions. Also the top and bottom boundaries of the tank are at such a distance that, according to analysis by Hazel (1972), any pairing after the first would be dampened. However, the initial growth of the shear layer and the first pairing should be largely unaffected.

3.2. *Secondary shear instability, convective instability, vortex dislocation, tubes and knots, and vortex tearing*

A shear-induced secondary instability commonly develops along the braid region between two Kelvin–Helmholtz vortices. As observed in figures 6(*m*), 7(*j*), 8(*l*), and 11, there can be anywhere from one to five or six such small Kelvin–Helmholtz-type vortical structures between two primary vortices. Except for the smaller size, these vortical structures are very similar to the primary Kelvin–Helmholtz structures in both appearance and dynamics, exhibiting similar roll-up and pairings. Several previous works have provided evidence for this type of secondary instability. Thorpe (1968) has reported observing this instability in his tilting tank experiments and depicts its

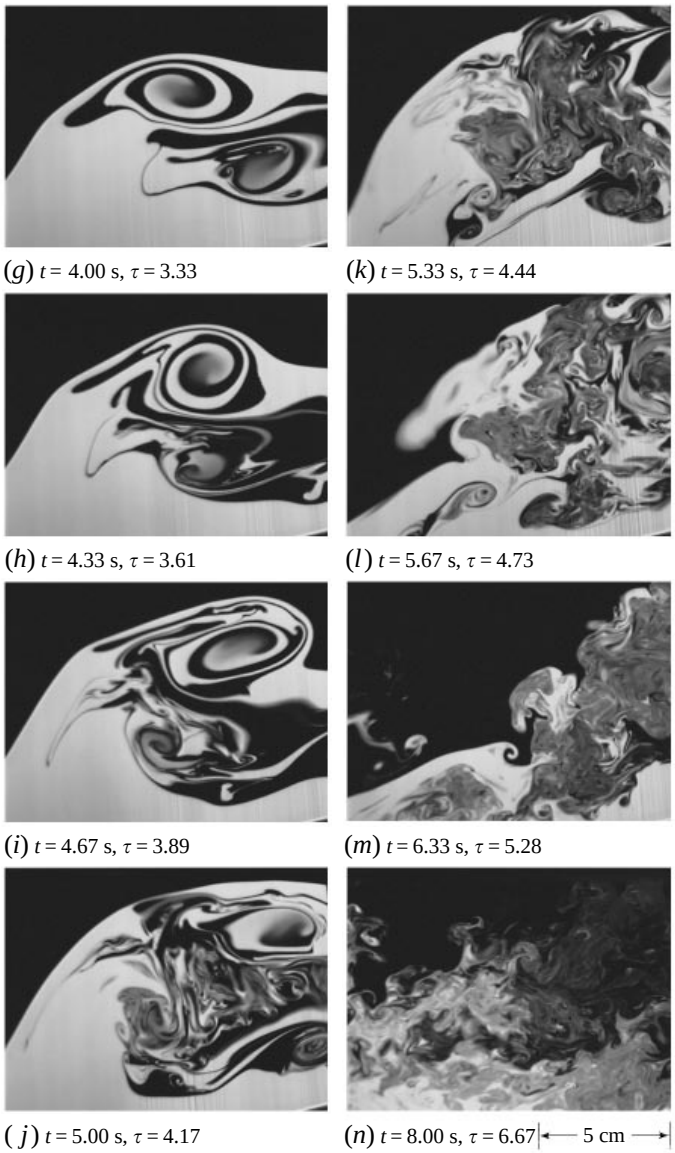

FIGURE 6. Side views showing the roll-up, pairing, and breakdown of the Kelvin–Helmholtz vortices in a weakly stratified two-dimensional mixing layer with $Re = 2150$ and $Ri = 0.012$. The time label for each image is from the onset of the Kelvin–Helmholtz instability. τ is time in seconds normalized by the shear-layer characteristic time $\lambda_{KH}/\Delta U_m/2)$. $\Delta\rho = 0.005$, tilt angle = 16°. Scale is at the bottom right of the image.

appearance in a drawing in his 1987 paper. Other investigators, such as Patnaik, Sherman & Corcos (1976), have also speculated on the possibility of its existence in stratified mixing layers. And the three-dimensional numerical simulations of stratified shear layers by Staquet & Riley (1989) have also identified the existence of these secondary spanwise Kelvin–Helmholtz modes.

The presence of the secondary shear instability in a stratified mixing layer and its absence in a homogeneous one is clearly due to baroclinic vorticity generation in the stratified flow, given by the source term $-(g/\rho_o)\,\partial\rho/\partial x$ in the vorticity equation. In a

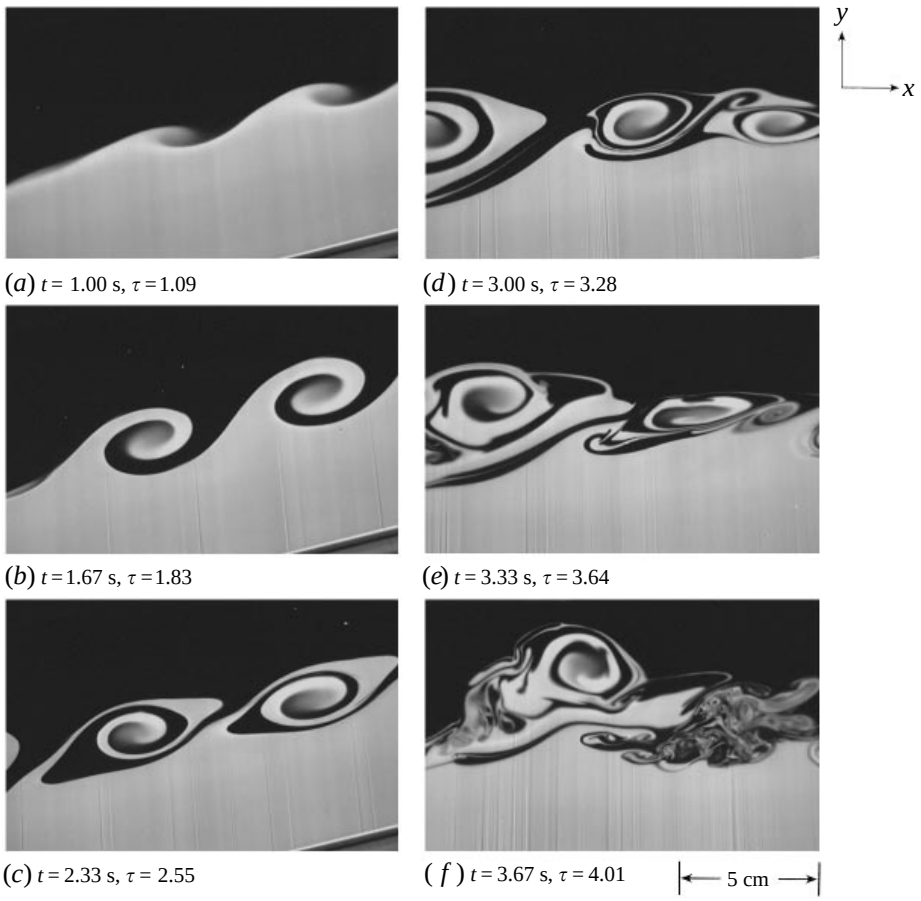

FIGURE 7 (*a–f*). For caption see facing page.

spatial homogeneous mixing layer, there is no new generation of vorticity down-stream of a splitter plate, but only advection and diffusion. In a stratified mixing layer, however, baroclinic vorticity generation remains active during roll-up and has a local maximum around the stagnation point in the braid (where $\partial\rho/\partial x$ is at a local maximum). Along the braid, the local shear induced by this mechanism coupled with the locally thin interface created by the strain field of the primary vortices can result in a low enough local Richardson number to allow a Kelvin–Helmholtz-type instability. For example the local Richardson number around the braid in figure 8(*i*), just before the appearance of the secondary braid instability, is estimated to be around 0.06.

The conditions under which the secondary instability of the baroclinic layer can grow have been explored in detail by Staquet (1995). In that work a heuristic argument, based on a theoretical framework by Dristschel *et al.* (1991), indicates that even a weak strain field imposed around the stagnation point by the primary Kelvin–Helmholtz vortices would prevent the secondary instability from strongly amplifying. The strain field compresses the baroclinic layer in the direction normal to it and has a stabilizing effect on any perturbation. Secondary instability grows if this strain field is significantly weakened. In the experiment of figure 8 two things are observed to weaken the braid strain field: the presence of a strong subharmonic component, which reduces the strain

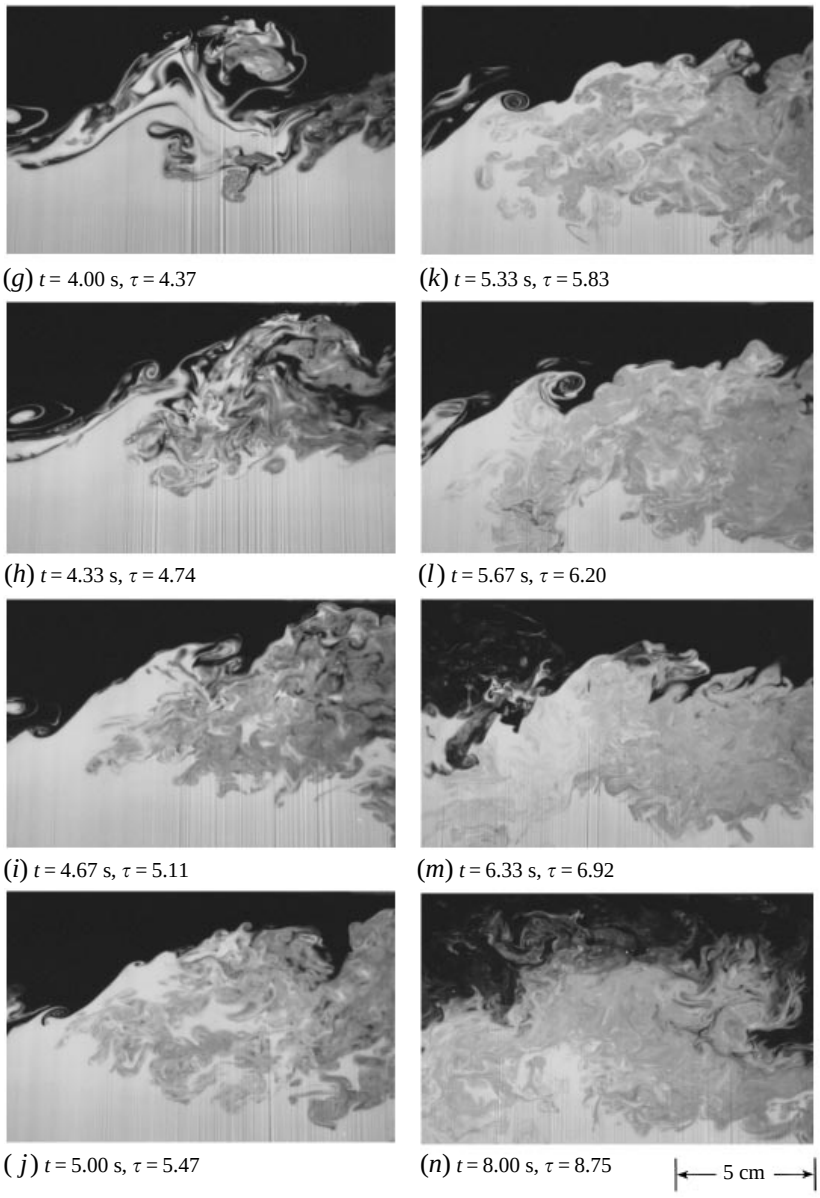

FIGURE 7. As figure 6 but in a stratified two-dimensional mixing layer with $Re = 2020$ and $Ri = 0.022$. $\Delta\rho = 0.01$, tilt angle = 16°.

rate in the baroclinic layer between two sets of pairing vortices; and the breakdown of the primary Kelvin–Helmholtz vortices, which allows the advection of vorticity into the stagnation-point region, disrupting the pure strain flow. Once the stabilizing strain field is suppressed, the secondary instability grows rapidly. If the conditions in the stagnation-point region of figure 8(*j*) after the breakdown of the Kelvin–Helmholtz vortices can be thought of as strain-free, a linear disturbance would grow by a factor of the order 10^5 by frame 8(*k*) in which the secondary instability is first visually identified. The small scale of the secondary instability is consistent with the local scale of the interface on which it develops. Note in figure 11(*d*) that the secondary instability

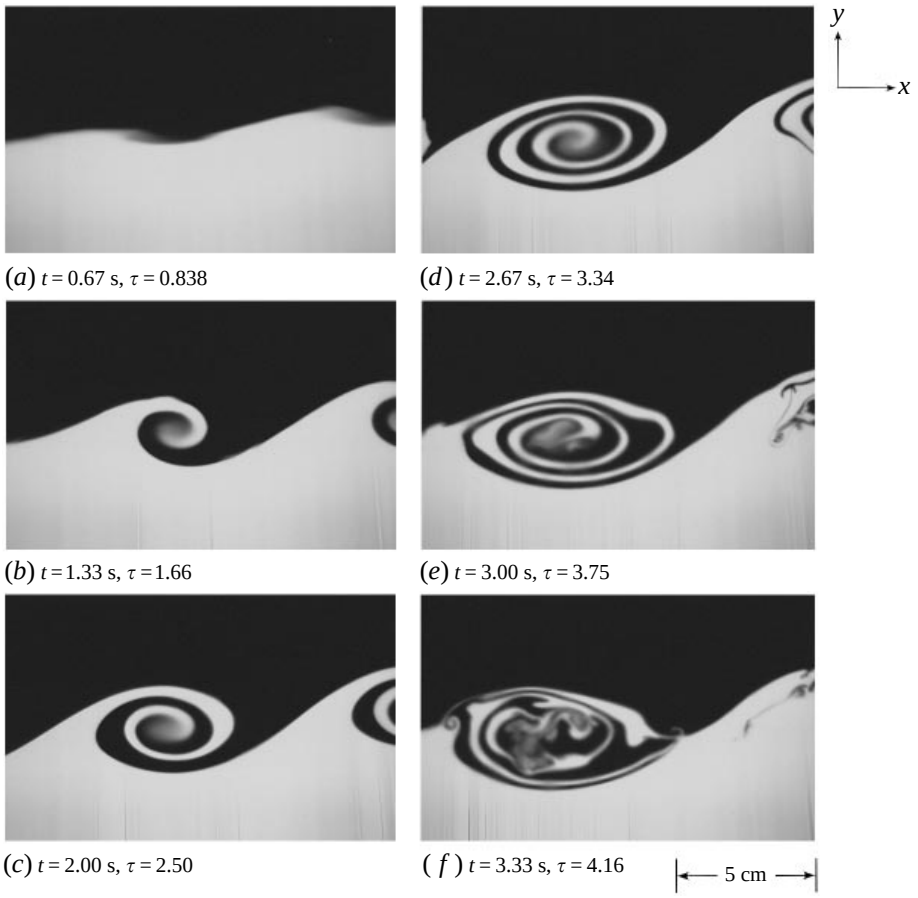

FIGURE 8 (*a–f*). For caption see facing page.

can repeat itself, creating even smaller tertiary structures (arrowed) between a pair of secondary vortices. This behaviour raises a very interesting question as to whether this cascade can continue as the Reynolds number of the mixing layer increases.

A gravitational instability of the Taylor–Rayleigh type (Thorpe 1971, 1985; Klassen & Peltier 1985; Schowalter *et al.* 1994) are often found within the statically unstable regions of the Kelvin–Helmholtz core, which consists of heavy and light fluid wrapped in a spiral roll. Where heavy fluid is found on top of light fluid, convective instabilities may amplify due to gravity. In the current experiments, the three-dimensional finger form (as seen in figure 8*f* and arrowed in 11*b*) as well as the usually reported two-dimensional convective rolls (as seen in the plan view of the shadowgraph in figure 12*f*, marked 'A') are observed. The Rayleigh number is given by $Ra = g\beta d^4/\nu D$, where d and $\rho_o\beta$ are the vertical scale and the density gradient at the centre of the statically unstable layer, respectively. In figure 8(*d*) the topmost unstable layer (the earliest unstable layer created in the core) has a Rayleigh number of about 1.4×10^5 with an estimated error of $\pm 0.3 \times 10^5$ (d is measured using a density profile through the layer). The growth rate of the unstable disturbances is given by $(gk\Delta)^{1/2}$ (Taylor 1950). In another experiment with the same parameters (figure 12), an instability is observed with a non-dimensional wavenumber of $k = 2\pi d/\lambda \approx 0.9$, giving a growth rate of around 3 s^{-1}. Between the time the first statically unstable layer is created and the time a Rayleigh–Taylor instability is first observed (figure 12*f*), the disturbances would have

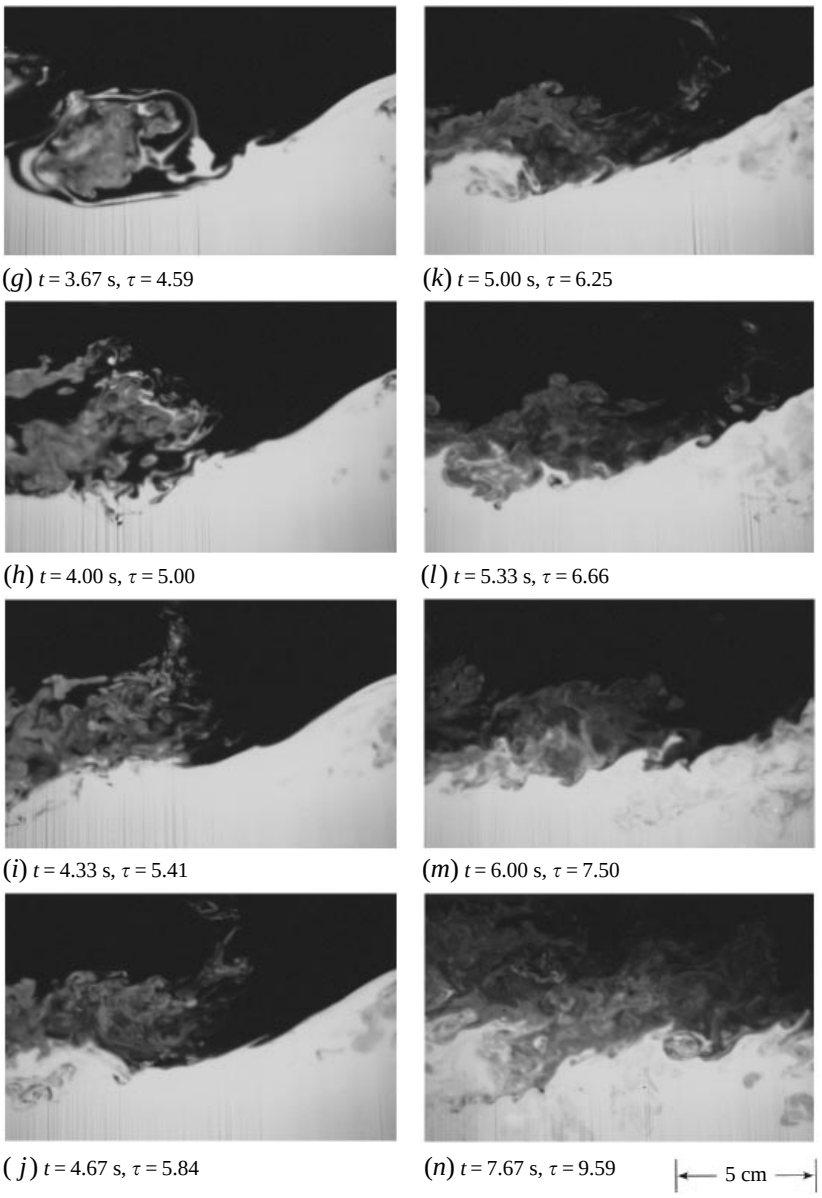

FIGURE 8. As figure 6 but in a stratified two-dimensional mixing layer with $Re = 2010$ and $Ri = 0.043$. $\Delta\rho = 0.02$, tilt angle = 8°.

amplified by a factor of 220. The scale of the instability $\lambda_{RT}/\lambda_{KH} = 0.13 \pm 0.1$, λ_{RT} being the wavelength of the counter-rotating longitudinal instability and λ_{KH} the wavelength of the Kelvin–Helmholtz instability, is consistent with Thorpe's (1985, figure 5) measurements of between 0.10–0.13.

A plan view of the interface between the top and bottom layers (figure 13) reveals a striking feature. Although the flow is generated in a very low-disturbance environment, the resulting spanwise vortices are often not perfectly two-dimensional. The picture of the flow is reminiscent of patterns in desert sand dunes – the structures in general are spanwise but exhibit random defects or dislocations of the

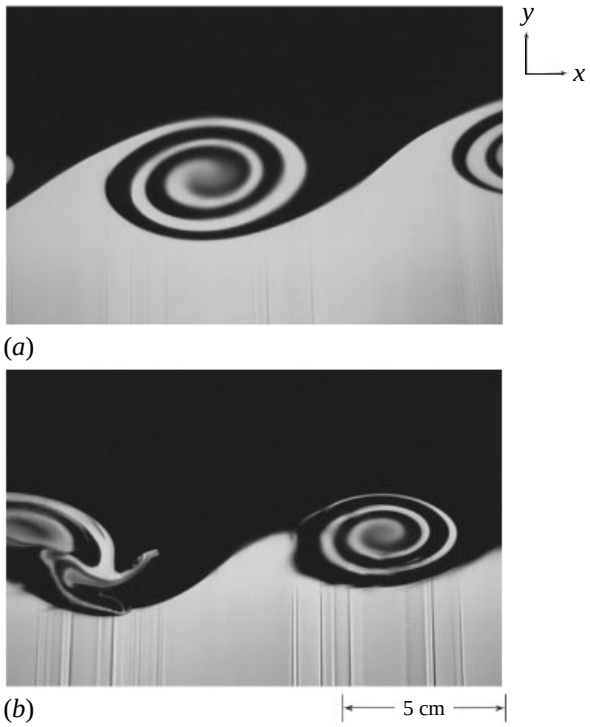

FIGURE 9. Side views of the Kelvin–Helmholtz vortices at the climax state for two Richardson numbers. (*a*) $Re = 2010$ and $Ri = 0.043$, (*b*) $Re = 1900$ and $Ri = 0.079$.

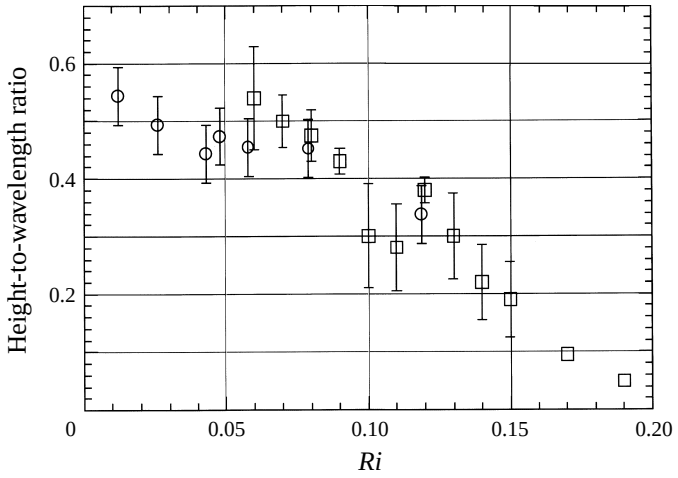

FIGURE 10. The ratio of the maximum Kelvin–Helmholtz roller height (at climax state) to wavelength *vs*. Richardson number. The error bars represent typical data scatter of different realizations at the same experimental conditions. ○, Present investigation; □, Thorpe (1973).

Kelvin–Helmholtz vortices, similar to the observation in a high-Reynolds-number homogeneous mixing layer by Browand & Troutt (1980). In figure 12 it is observed that the Kelvin–Helmholtz structures, in the early stages of roll-up, tend to develop into separate interacting 'patches' in the plane of the shear layer. In the early stages, the visible length of the vortices usually does not span the whole width of the tank,

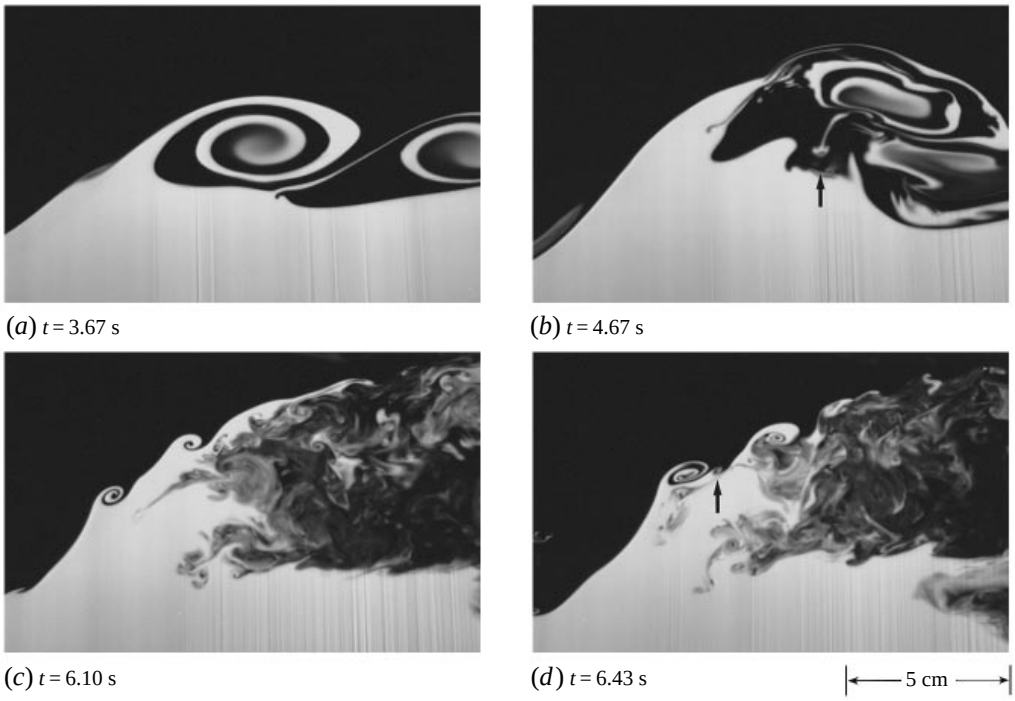

FIGURE 11. Side views showing secondary Kelvin–Helmholtz vortices in a stratified mixing layer with $Re = 2200$ and $Ri = 0.026$.

indicating the existence of regions with decreasing wave amplitude around the edges. The phase and the wavelength of the vortices in a patch sometimes slightly mismatch those in the neighbouring patches, resulting in vortices that appear staggered. This deviation from perfect periodicity has been attributed to the presence of a 'phase jitter', which arises from the amplification of subharmonic perturbations from the background noise (Ho *et al.* 1991). Since the background noise is random in the shear plane, its amplification could conceivably result in slightly different vortex evolution patterns in different regions of the mixing layer. Consequently, vortex dislocations form in the regions where the vortices try to negotiate the phase and wavelength mismatches. Examples of dislocations are illustrated in figures 12(*a*) and 12(*b*) (marked 'B' and 'C'). Thorpe (1985) has described similar-looking structures, which he calls 'knots', in some detail. Perhaps it is not quite clear that knots and dislocations can be categorized as different types of structures. The tubelike structures (marked 'D', figure 12*d*) are also routinely observed by Thorpe (1985). The most important observation about these structures, whether they are categorized as vortex dislocations, tubes, or knots, is that the breakdown of the Kelvin–Helmholtz vortices contains considerably more random small-scale structures where they are present, an observation also made in Thorpe & Holt (1995).

Figure 14 shows an interesting situation in which a small Kelvin–Helmholtz vortex is caught within the strain field of two larger vortices. The high strain rate of the larger vortices causes the small vortex to stretch along the principle axis of strain and flatten along the normal direction, causing it to collapse. This type of 'vortex tearing' is rarely observed and probably does not contribute much to the overall turbulent processes, although it is possible that this phenomenon happens more frequently at smaller scales, which has not been recorded through flow visualization.

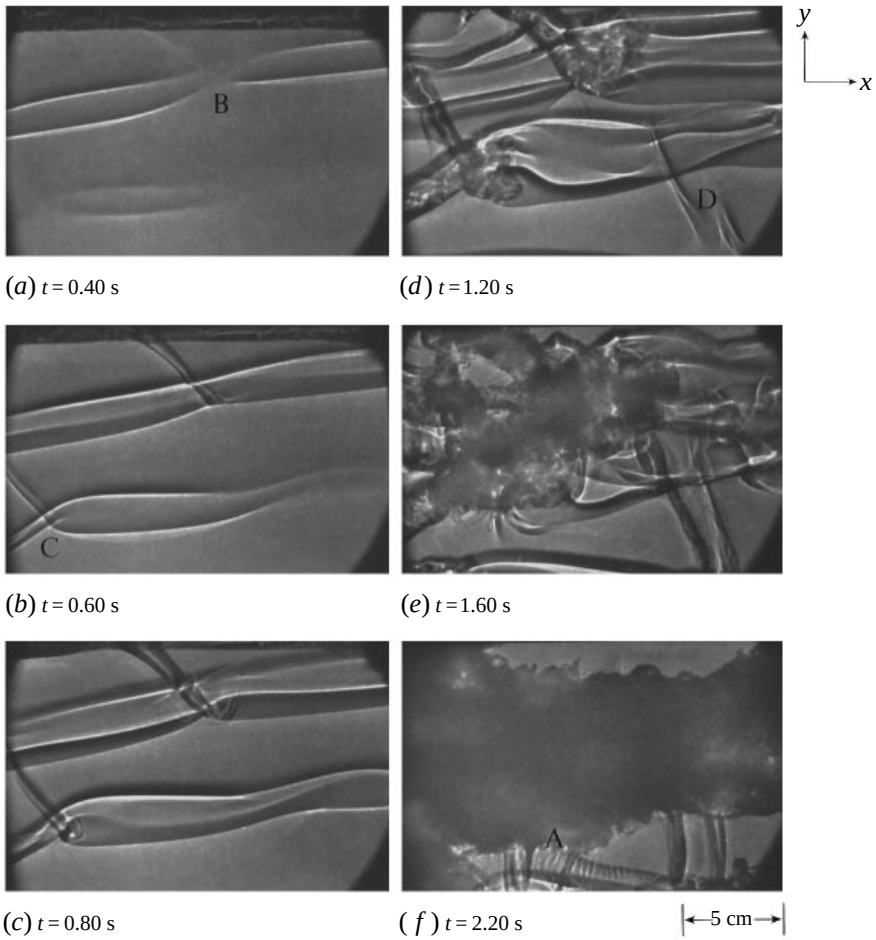

FIGURE 12. Plan-view shadowgraphs of a two-dimensional stratified mixing layer with $Re = 2010$ and $Ri = 0.043$.

3.3. *Material interface stretching measurements*

An important difference among the mixing layers presented in figures 6–8 is the fact that the large-scale vortices in the most-stratified case (figure 8, $Ri = 0.043$) did not pair. Large-scale vortex pairing is usually considered the dominant process contributing to the overall growth in the vertical extent of the mixing layer, a large-scale process upstream of events generally associated with small-scale molecular mixing. Observations of the pairing process in figure 6 and 7, however, illustrate much more than a large-scale rotation of two vortices around a common centre. As two vortices are brought closer together towards mutual interaction, the fluid interface within the interacting region experiences complex stretching and folding, resulting in a highly convoluted fluid surface separating light and heavy fluid (as seen in figures 6*g–i* and 7*e–g*). This interface stretching and folding (reminiscent of kneading of bread-dough) does not resemble any known dynamical flow instability and seems to be mainly a kinematic phenomenon. This process resembles flows that are considered chaotic, similar to those examined in the numerical calculations of two-dimensional mixing

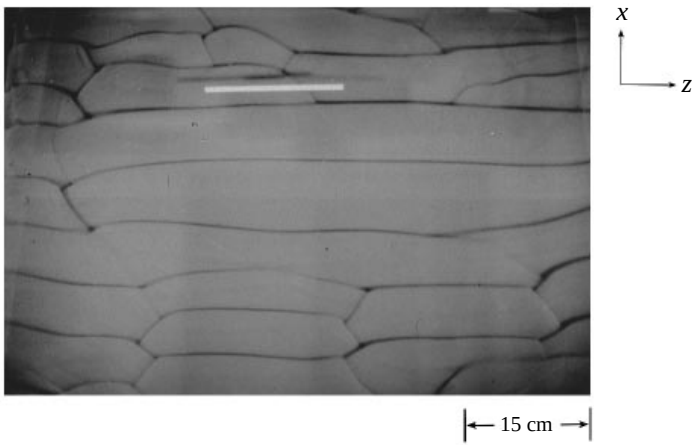

FIGURE 13. Plan view showing the 'branching' or 'dislocation' patterns in the initial roll-up of the Kelvin–Helmholtz instability. The bottom layer is premixed with a high concentration of dye so that the illumination does not penetrate the interface more than a few millimetres. The black lines represent the front edge of the Kelvin–Helmholtz vortices that would form shadow when illuminated from the top. $Re = 2800$, and $Ri = 0.040$. The white band at the top is a 6 in. scale.

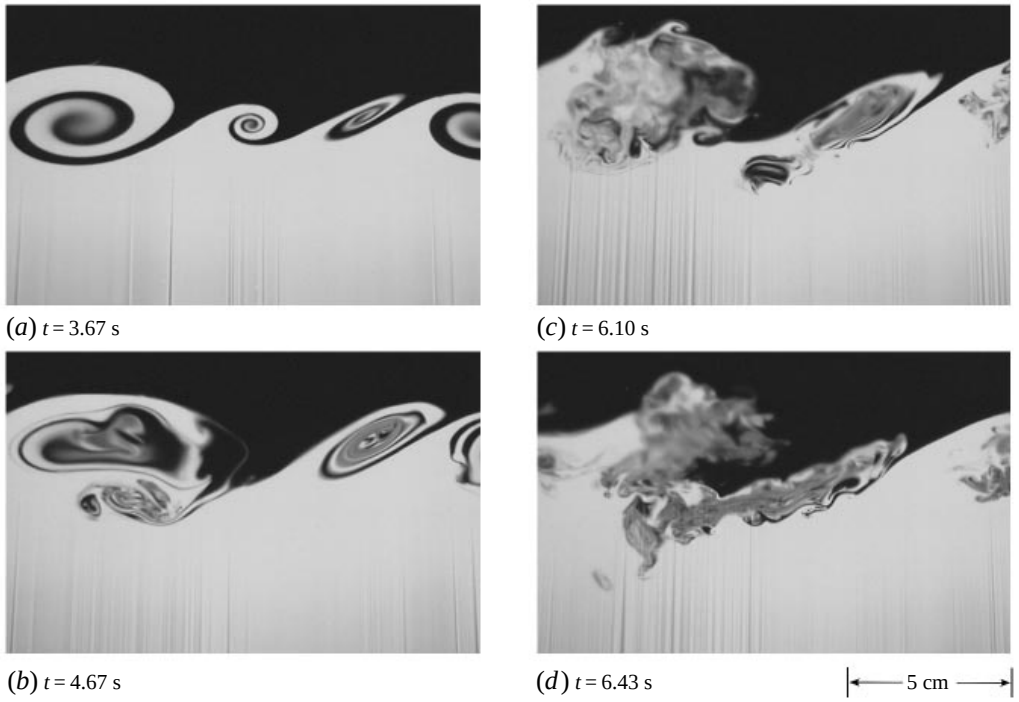

FIGURE 14. Side views showing vortex tearing in a stratified mixing layer with $Re = 1900$ and $Ri = 0.048$.

layers by Jimenez & Martel (1991, figure 10) and Min (1994, figures 5.5 and 5.13). One feature of a chaotic flow is the presence of Smale horseshoe functions (Chien, Rising & Ottino 1986), which involve the stretching and folding of a square onto itself. A similar behaviour in the material line shapes can be seen in figure 6(*h–j*). In a chaotic flow the length of a material line grows exponentially in time, implying better fluid

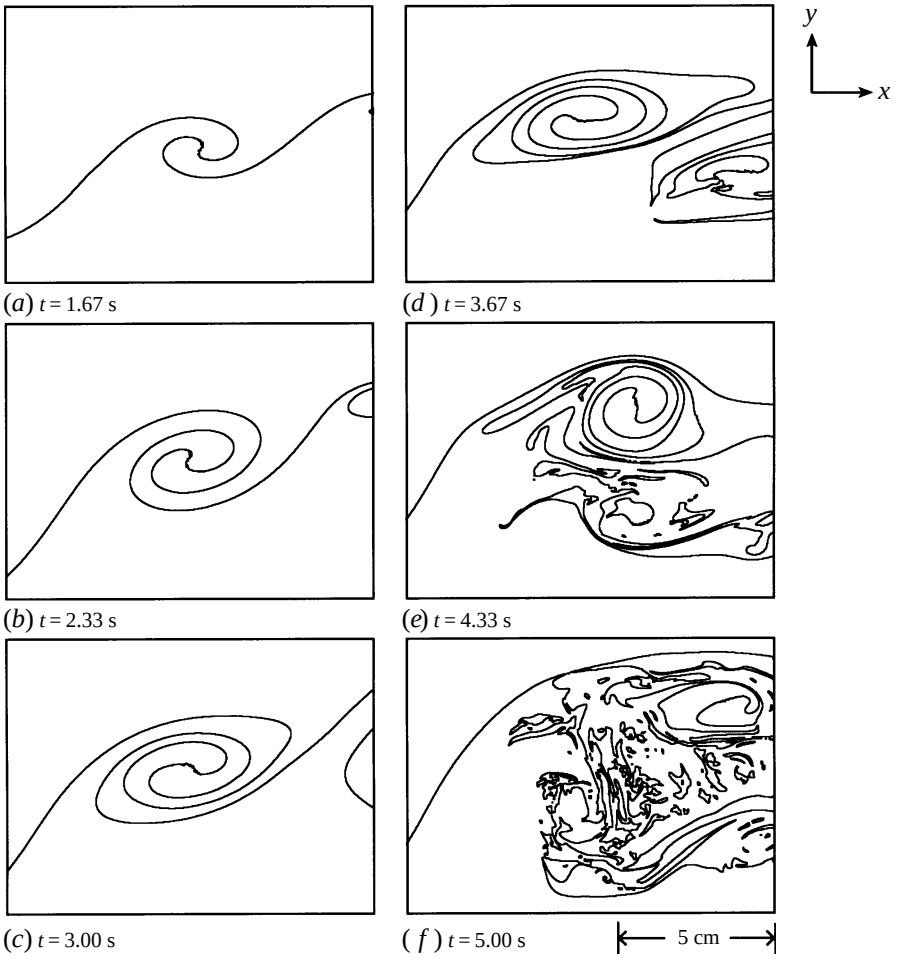

FIGURE 15. Images showing the material interfaces where diffusion is active. These images are equivalent to samples from figure 6 where $Re = 2150$ and $Ri = 0.012$. The time label for each image is from the onset of the Kelvin–Helmholtz instability.

'stirring' than in non-chaotic flows by generating a larger amount of diffusive surface separating the two layers of fluids.

The measurement of the growth of the material interface length between the top and the bottom fluids is carried out by digitizing each LIF image, thresholding it to the intensity that represents fluid of density $(\rho_{bottom}+\rho_{top})/2$, finding the edges of the thresholded images, and measuring the total length of the interfacial lines, which is proportional to the total diffusive interfacial area (assuming a nominal two-dimensionality). A sample of the processed images is presented in figure 15 (the same experiment as figure 6), and the result of the measurement is presented in figure 16. The abscissas represent the time in seconds normalized with the shear layer characteristic time $\lambda_{KH}/(\Delta U_m/2)$, λ_{KH} being the wavelength of the Kelvin–Helmholtz instability. The ordinates (log in figure 16*a* and linear in 16*b*) represent the material interface length, normalized by the initial value before the Kelvin–Helmholtz roll-up. Only two Kelvin–Helmholtz wavelengths are sampled in each case, in order to capture pairing

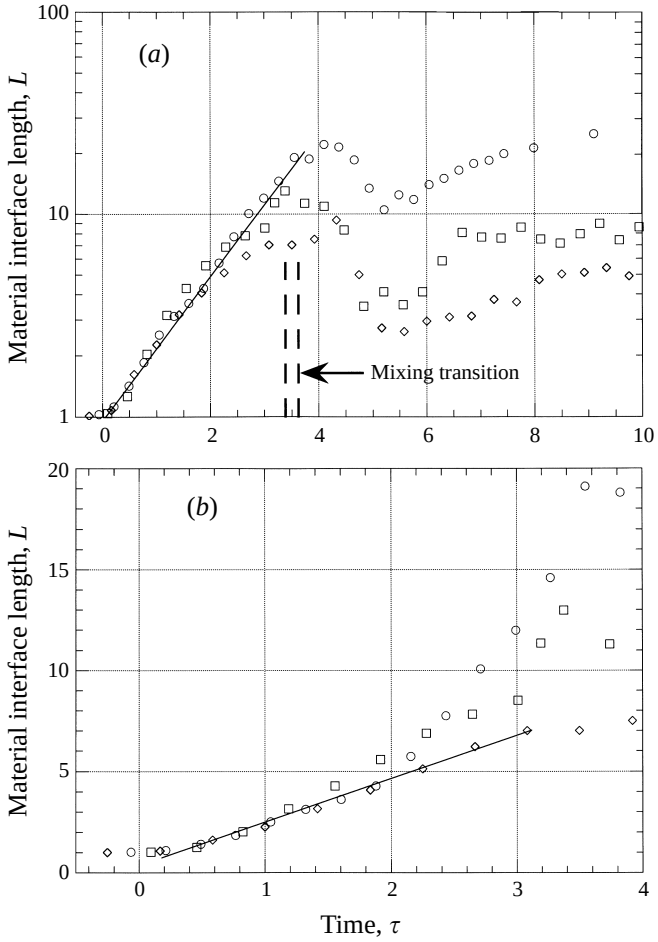

FIGURE 16. Material interface generation in the evolution of mixing layers. The material interface length is normalized with the original interface length before any instability, and time with the shear layer characteristic time $\lambda_{KH}/(\Delta U_m/2)$. ○, $Ri = 0.012$; □, $Ri = 0.026$; ◇, $Ri = 0.043$.

but at the same time maximizing optical resolution. Strong interactions of pairing vortices result in higher material interface growth in the cases with lower stratification. In the $Ri = 0.012$ case the material interface stretches to about 20 times its original length before the onset of small-scale three-dimensional motions (figure 6*j*). In figure 16(*a*) it can be seen that growth of the material interface for the two cases with pairings does indeed follow an exponential curve, whose slope of about 0.8 is the finite-time Lyapunov exponent defined by

$$\beta = \frac{1}{\tau}\ln\left[L(\tau)/L(0)\right],$$

where L is the measured interfacial length and τ is the time in seconds normalized with the shear layer characteristic time $\lambda_{KH}/(\Delta U_m/2)$. The material interface growth for the higher-Ri case of 0.043, however, appears to be linear (figure 16*b*). The main difference is that the vortices in this case do not go through pairings as in the two lower-Ri cases. The dips in the material interface length after the mixing transition are due to the fact that fluid mixing tends to smear out the sharp interfaces created in the roll-up and

chaotic stretching processes. At this point in time, the level of mixedness in the mixing layer is observed to increase sharply.

After the onset of three-dimensional small-scale motions, a prominent level of mixedness is observed not only within the cores of the Kelvin–Helmholtz vortices but also in the area with abundant interface stretches and folds. The present experimental observations highlights some crucial steps in the chain of events that leads to an efficient mixing transition. The pairing kinematics of the two-dimensional large-scale structures could be important to the mixing processes, not only by directly creating a large increase in the diffusive interface across which fluids can mix in the molecular sense, but also by effectively 'stirring' the fluids so that once the small-scale transition takes place, the fluids may be mixed more efficiently.

Some discussions regarding the measurement method of the material interface length are warranted. It is possible that just before the small-scale transition, the material interface contains stretches and folds of the scales that cannot be resolved by the recording system, and thus the interfacial length might be higher than measurements suggest. And since the definition of the interface is based on a chosen pixel intensity value (threshold value), small errors in the attenuation correction would translate into errors in the interface identification, a potentially serious problem after the mixing transition. A measurement after the mixing transition is also highly sensitive to the choice of threshold value (although there really is no physical reason to choose any other threshold value except for 0.5, which represents the density of mixed fluid containing equal parts of top and bottom fluid). Thus the measurements could be seriously unreliable after the mixing transition ($\tau > 4$ in figure 16). However, the above discussions about the significance of pairings on the material interface growth are not in any way invalidated by these errors since our conclusions are based wholly on data taken before the mixing transition.

3.4. *Mixing measurements*

To determine the effect of stratification on the overall growth of the mixing layer, the 'total yield' of mixed fluid is measured at various Richardson numbers, keeping Reynolds number roughly constant. The procedure, as described in §§2.5 and 2.6, consists of taking LIF images of the mixing layer after the turbulent transition and relaminarization. The images obtained are corrected for the horizontal Gaussian profile drop-off and the vertical laser dye attenuation, before the amount of the mixed-fluid thickness δ_m is calculated (see Appendix). In the $Ri = 0.16$ case, there is no Kelvin–Helmholtz roll-up; therefore, the measured mixing reasonably represents typical mixing due to surges returning from the endwalls and standing wave motions. This amount of expected error is integrated into the error bar used with the data.

Figure 17 shows that the ability of the mixing layer to mix fluids is drastically reduced as the Richardson number increases. The reason for this reduced mixing is a combination of the reduction in the volume of fluid entrainment into the Kelvin–Helmholtz vortices (see figure 10), the smaller entrainment ratio of the heavier bottom fluid into the cores (see figure 9), the reduced frequency of pairing of the large-scale structures (discussed in §3.1), and the subsequent arrest of turbulence as the stabilization effect of stratification eventually relaminarizes the flow. Plotted along with the current data are comparable data from Koop & Browand (1979), who performed their experiments in a water tunnel and measured the fluid mixing with a conductivity probe, at their last measuring location after the mixing layer has restratified and does not produce significantly more mixing.

It is hard to gauge exactly what share of the reduction in mixing each mechanism is

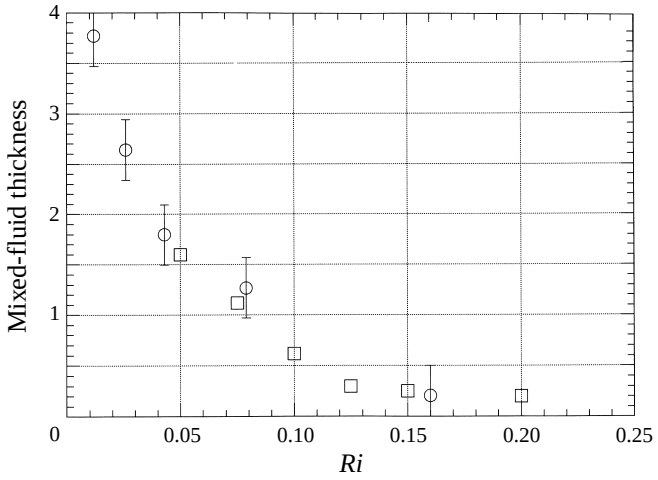

FIGURE 17. The mixed-fluid thickness normalized by the velocity thickness δ_v *vs.* Richardson number. The Reynolds numbers for the experiments are all around 2000. ○, Present investigation; □, Koop & Browand (1979).

responsible for as stratification increases. It seems safe to say that between $Ri = 0.012$ and 0.043, where the drop in mixing is sharpest, the main effect is the reduction in pairing and the corresponding reduction in material interface generation. The size of the Kelvin–Helmholtz vortices remains roughly constant within this Richardson number range (figure 10), and the entrainment ratio only decreases from about 1 to 0.8; therefore, these two effects could not have accounted for much more than a fraction of the twofold reduction in mixing. Perhaps not coincidentally, the maximum interfacial length decreases a little more than twofold between $Ri = 0.012$ and 0.043 (figure 16). For the Richardson number range of 0.043 to 0.16, on the other hand, there is very little pairing at all but a fourfold reduction in the size of the large-scale vortices and a twofold reduction in their fluid entrainment ratio. Therefore, within this Richardson number range the measured sevenfold reduction in mixing seems to be due mainly to the stabilizing effect of stratification on the roll-up and fluid entrainment of the large-scale Kelvin–Helmholtz vortices.

4. The mixing layer with cross-shear

4.1. *Co-rotating streamwise instability*

The introduction of a critical level of cross-shear to a plane shear layer results in a new type of 'co-rotating' streamwise vortices in the braid region of the primary Kelvin–Helmholtz instability. Flow visualizations in figures 18–22 illustrate different qualitative aspects of this phenomenon. The visualization method used in the plan view of figure 18 is the same as that for figure 13 (see §2.4 and the caption of figure 13). The dark lines are shadows formed by illumination from above and coincide with the right-hand edges of vortical structures when viewed from the side (figures 6–8). The main shear gives a vorticity component in the negative z-direction, and the cross shear one in the negative x-direction. The primary Kelvin–Helmholtz instability appears as expected, with the primary vortices aligned along the z-axis (spanwise direction). With the introduction of cross-shear, the general characteristics of the Kelvin–Helmholtz vortices do not seem to be affected in any significant way. But along the braid region, very organized streamwise streaks, oriented roughly perpendicular to the main

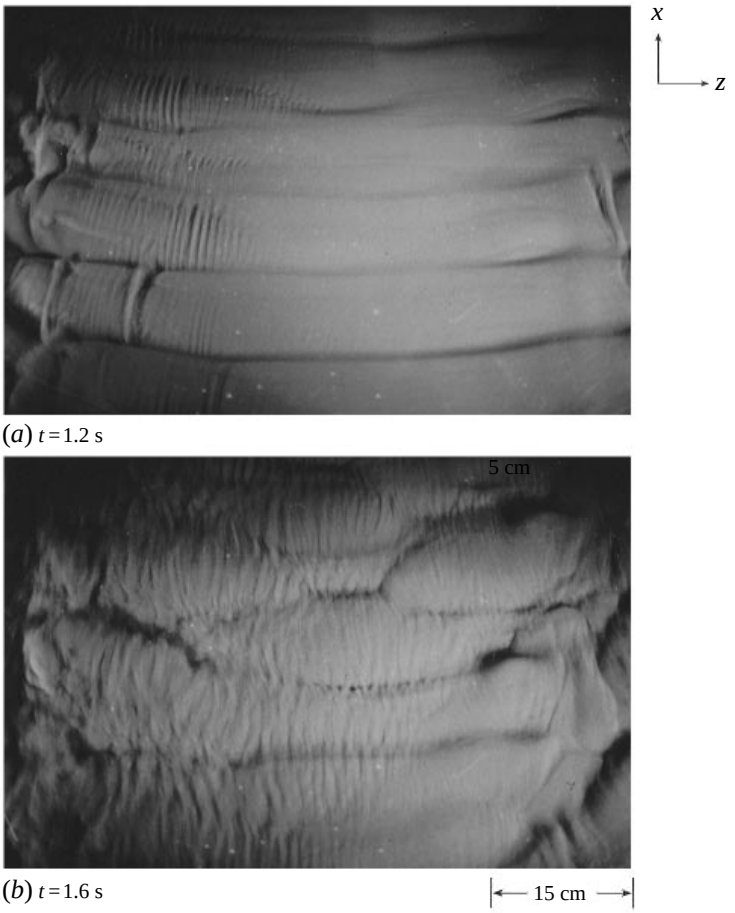

FIGURE 18. Plan views of a mixing layer with cross-shear. Streamwise streaks develop along the braid and increase in scale as they evolve. The time label is after the onset of the primary Kelvin–Helmholtz instability. Cross-shear is introduced 4 s after the main shear, shortly after the onset of the primary Kelvin–Helmholtz instability (at 3.9 s). *Re* and *Ri* of the main shear are 2800 and 0.034, respectively. The magnitude of the cross-shear is about 21.5% that of the main shear. The sidewalls are about 3.5 cm away from the edges of the pictures.

vortices, are observed to develop (figure 18*a*). The length scale of the streaks is initially about 0.75 cm, an order of magnitude lower than that of the primary vortices, which have a wavelength of about 7.5 cm. As the mixing layer develops, the length scale of the streamwise streaks increases, seemingly going through successive doublings in scale (figure 18*b*). Eventually, the mixing layer goes through turbulent transition in which a large increase in random small-scale three-dimensional motions is observed. Figure 19 is also a plan-view visualization but using the shadowgraph method. The top dark/bright band coincides with the right-hand edge of a vortical structure when viewed from the side (see figure 8*b*). The faint bright band right underneath approximately marks the centre of the vortex, and the dark/bright band right below represents the left-hand edge. Note that the lower dark/bright band is not recorded in the flow visualization used in figure 18. Again streamwise streaks are observed in the braid region of the Kelvin–Helmholtz instability. Also observed is the helical pairing of the primary vortices, a three-dimensional instability mode of the spanwise vortices identified by Pierrehumbert & Widnall (1982). The top and bottom vortices initially

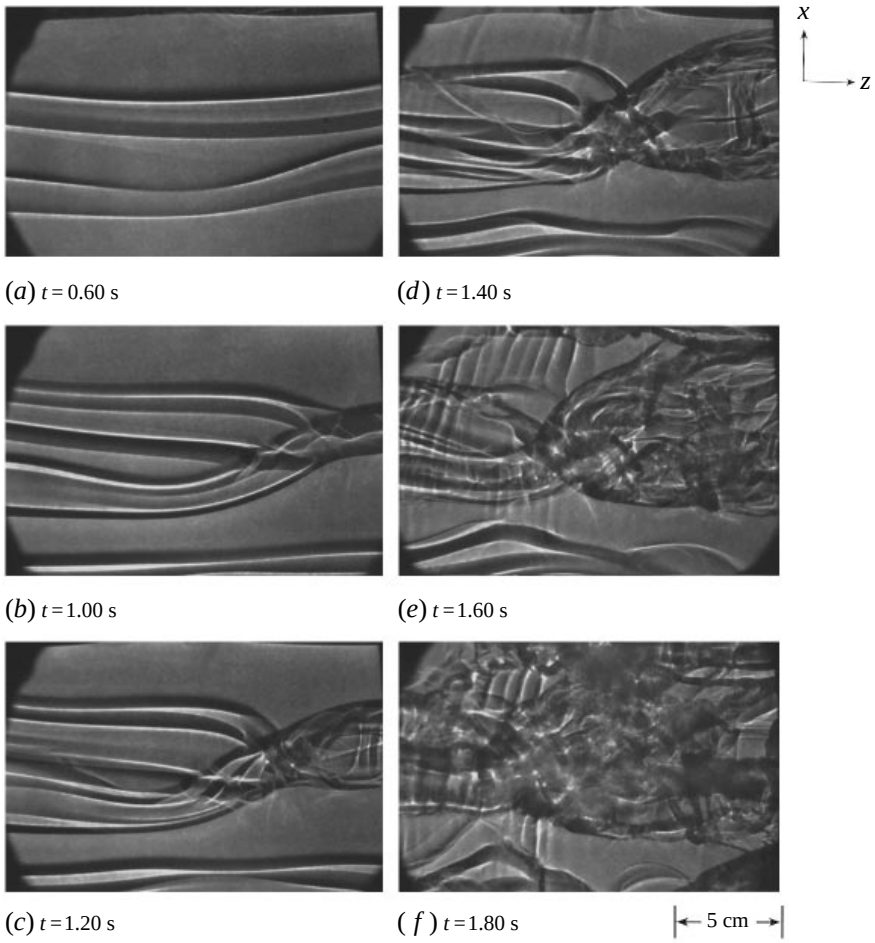

FIGURE 19. Plan-view shadowgraphs of a stratified mixing layer with cross-shear. $Re = 1900$ and $Ri = 0.048$. Cross shear is about 32.5% of the main shear. The time for each image is from the onset of the primary Kelvin–Helmholtz instability. The sidewalls are about 29 cm away from the edges of the pictures.

pair only locally (figure 19*b*), but the interaction spreads laterally and eventually involves the entire span of the vortices.

The y–z view or a cross-section of the braid region illuminated by a laser sheet (figure 20) clearly shows that the streaks are in fact structures of concentrated vorticity and that they are of the same sign everywhere. Qualitatively, the streamwise vortices exhibit similar roll-up and pairing dynamics as the primary Kelvin–Helmholtz vortices. Figure 21 is a sequence of pictures showing the pairing of two streamwise vortices. Quantitatively, the length scale and time scale of the secondary vortices are also roughly of the same order as those of the primary vortices. We use as length scale the instability wavelength normalized by the local density thickness and as time scale the pairing time of two vortices normalized by the overturning time scale $\lambda/(\Delta U/2)$. The average wavenumber of the streamwise vortices is 0.48 with a standard deviation of 0.05, and the average ratio of the streamwise-to-primary pairing time scale is 1.2 with a standard deviation of 0.2. It is normal for the streamwise vortices to pair twice or three times, eventually making their sizes comparable to those of the primary vortices,

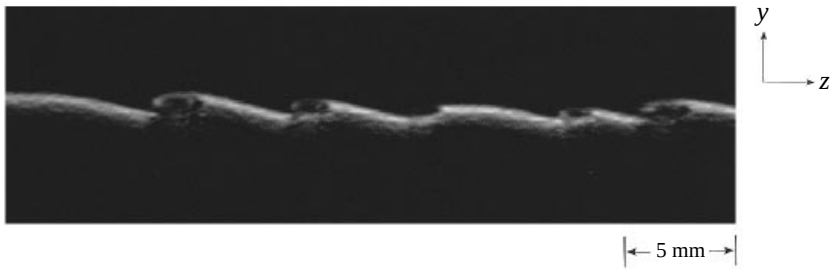

FIGURE 20. A cross-section of the streamwise streaks showing the co-rotating streamwise vortices. The image is taken 1.50 s after the onset of the primary Kelvin–Helmholtz instability. Cross-shear is introduced 4 s after the main shear, around the time of the onset of the primary Kelvin–Helmholtz instability (at 4.1 s). *Re* and *Ri* of the main shear are 1880 and 0.09, respectively. The magnitude of the cross-shear is about 50% that of the main shear.

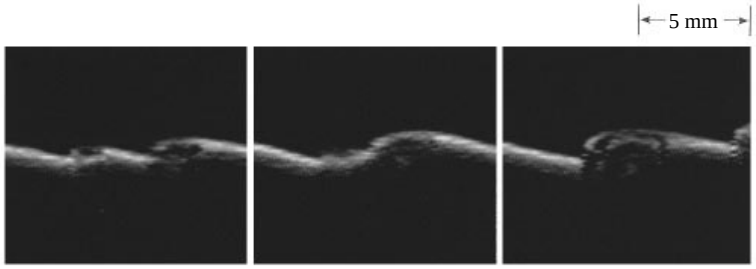

FIGURE 21. A sequence of pictures showing two co-rotating streamwise vortices in the process of pairing. The experiment is the same one as in figure 20. The times of the sequence are after the onset of the primary Kelvin–Helmholtz instability.

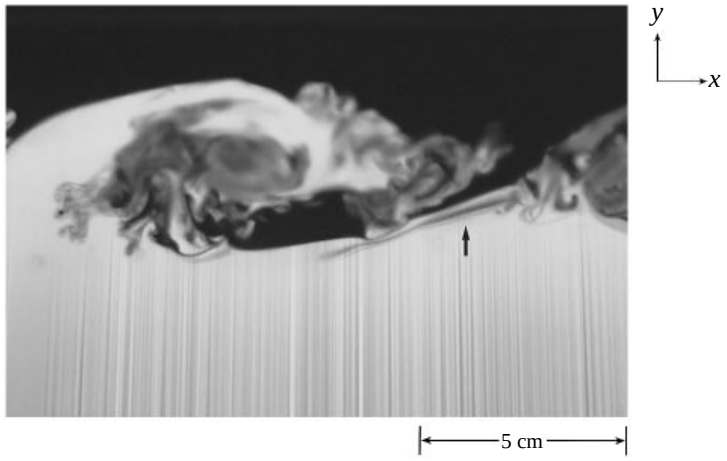

FIGURE 22. Side view of streamwise vortices in a mixing layer with $Re = 1950$ and $Ri = 0.046$. The magnitude of the cross-shear is about 25% that of the main shear.

which pair much slower. Figure 22 reveals a braid region layered in alternate dark and bright bands, indicating the spiral form of a streamwise vortex. From this view the streamwise vortex is seen to reside mainly in the braid region and does not extend across billows to the adjacent braid regions. The photograph of clouds in figure 23

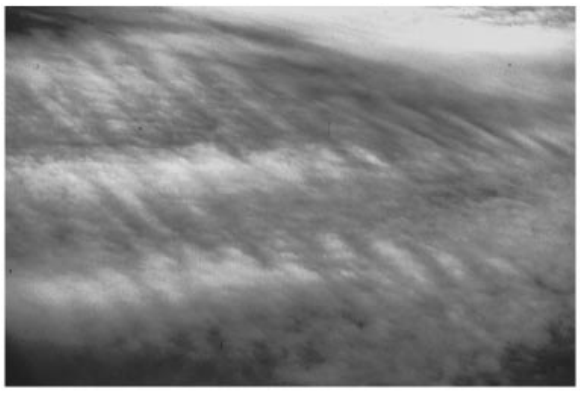

FIGURE 23. Cloud pattern showing large-scale spanwise rolls and small-scale longitudinal rolls similar to co-rotating streamwise vortices. The picture is taken using a 35 mm camera with a 210 mm lens, from an aircraft window at a 30° down angle. The aircraft was about 6000 ft above the clouds.

displays a pattern with long-wavelength bands in one direction, and smaller-wavelength bands in the perpendicular direction, raising a question about the possible existence of this type of instability in a wide range of conditions.

The above observations of the streamwise co-rotating instability lend enough insight to allow the construction of a simple conceptual model. The introduction of cross-shear essentially has the effect of imposing streamwise vorticity globally in the plane mixing layer. Around the stagnation point in the braid, the local flow field in the (x, y) plane is approximately a plane strain field that locally stretches and magnifies the streamwise vorticity, making a Kelvin–Helmholtz-type instability likely. The wavelength of the streamwise vortices is expected to scale on the local density thickness in the braid, which is about an order of magnitude lower than that of the primary shear layer. This heuristic argument is modelled after the stability and numerical analyses of Lin & Corcos (1984), which examine the development of counter-rotating streamwise vortices in the strain field of the braid by modelling the local flow field around the stagnation point with a plane strain field and imposing on that system a spanwise-sinusoidal distribution of streamwise vorticity. In §4 of that work, however, the authors examine a special case in which the wavenumber of the initial sinusoidal streamwise vorticity is zero, meaning that the imposed streamwise vorticity is basically a plane streamwise vorticity layer. They determine the stability characteristics of the strained vortex sheet and show that it exhibits roll-up and pairing dynamics similar to the unstrained case. This conceptual model, treating the co-rotating streamwise vortices as strained Kelvin–Helmholtz vortices, ignores the question of how the ends of the streamwise vortices interact with the primary Kelvin–Helmholtz structures. Nevertheless, the streamwise-to-primary length scale and time scale ratios of the co-rotating streamwise vortices (see §4.1) are consistent with the behaviour of the instability in a strained vortex sheet, which has a higher wavenumber and longer pairing time than the unstrained case (Lin & Corcos 1984).

It is important to point out that the streamwise vortices develop even when the cross-shear is too weak to become unstable by itself. For example in the experiment of figure 18, if the cross-shear were present alone, the Richardson number would be about 0.4, well above the critical number of 0.25. But with the stretching action of the braid strain field, the local length scale in the braid can get drastically smaller, and the local Richardson number can be reduced by an order of magnitude (of the order of 0.04), making a shear-induced instability likely. Therefore, one cannot think of the flow as

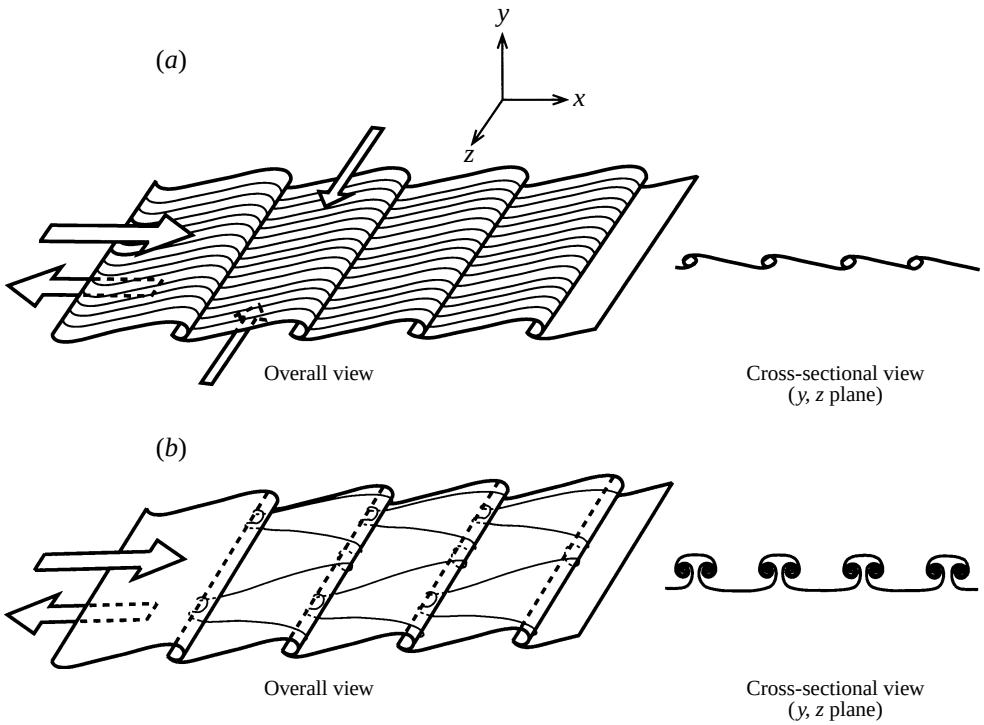

FIGURE 24. (*a*) A schematic showing the overall picture of a mixing layer with cross-shear. A cross-section of the streamwise streaks in the braid reveals they are 'co-rotating' streamwise vortices. (*b*) A schematic showing the overall picture of a mixing layer with the 'mushroom' type streamwise vortices.

two separate and independent sets of perpendicular Kelvin–Helmholtz instability superimposed upon each other. Rather, the streamwise vortices are manifestations of an instability of the Kelvin–Helmholtz braid. It is evident from figure 18 (see the rightmost streamwise structures between the second and third spanwise vortices from the bottom) that the streamwise instability first grows in the braid region but later extends towards the cores. The streamwise vortices are not the results of sidewall effects; they first appear in the middle of the tank (as in figure 19) as often as near the sidewalls (as in figure 18). Figure 24(*a*) shows the overall view of a mixing layer with cross-shear. Viewed from top, the streamwise vortices appear as streamwise streaks. These streamwise vortices are distinct from the counter-rotating type (Bernal & Roshko 1986), which would reveal 'mushroom' shapes in the (y, z) plane (see figure 24*b*), the wavelength of which would not increase because the mushroom structures do not pair.

4.2. *Convective instability and localized co-rotating streamwise vortices*

The co-rotating streamwise structures could easily be confused with the convective instability that usually presents itself in the form of streamwise counter-rotating vortices (Thorpe 1971). The two forms of instabilities are very similar in appearance, being mainly longitudinal and of much smaller wavelengths than the primary Kelvin–Helmholtz vortices. For the experiment in figure 18, convective rolls are ruled out because the visualization method is designed to visualize only the interface (see §2.4), and any convective instability would reside mainly inside the cores and not be visualized. Moreover, the length scale of the streamwise streaks in figure 18 is

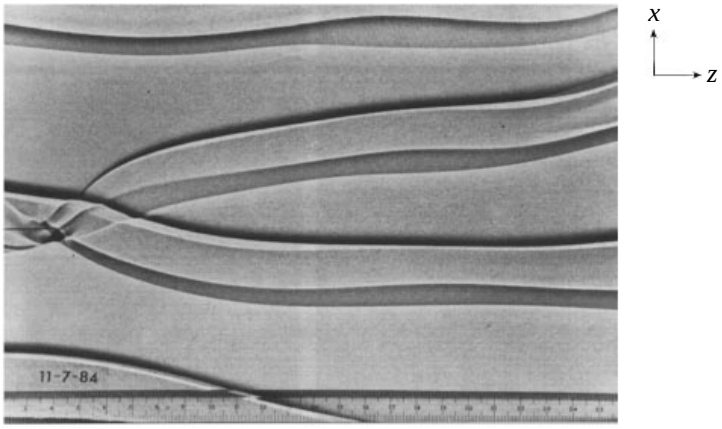

(*a*) $t = 3.18$ s

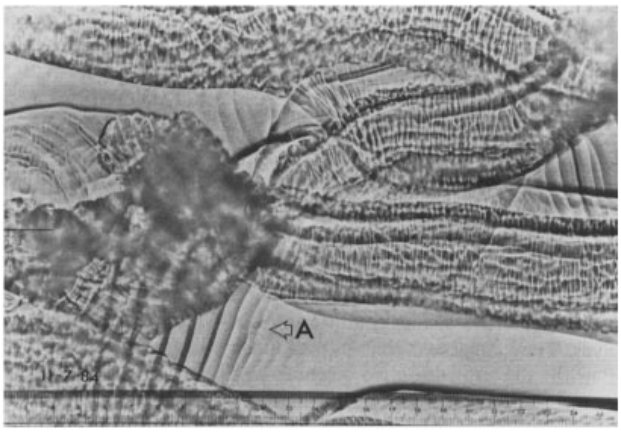

(*b*) $t = 3.47$ s

FIGURE 25. Plan-view shadowgraphs from figure 7 in Thorpe (1985) of a two-dimensional stratified mixing layer with $Re = 3900$ and $Ri = 0.059$ at the onset of Kelvin–Helmholtz instability. The times of the images are from the initiation of tilt. The onset of the main Kelvin–Helmholtz instability (from Thorpe's figure 3) is about 2.9 s after tilt. The scale is in cm. (Reproduced with the author's permission.)

consistent with that of Kelvin–Helmholtz-type structures (see the discussion in §4.1). The wavelength of any convective roll, according to data by Thorpe (1985) at the same flow parameters, would be about 1/3 that of the wavelength of the observed streamwise streaks. Convective instability can instead be observed in shadowgraphs, for example in figure 12(*f*), which visualizes through the whole depth of the fluid. The observed convective rolls (marked 'A') reside inside the cores and have a length scale consistent with the data by Thorpe (1985).

Figure 25 shows plan-view shadowgraphs of a two-dimensional stratified mixing layer with $Re = 3900$ and $Ri = 0.059$, reproduced from Thorpe (1985). In the vicinity of a three-dimensional localized pairing, streamwise streaks (marked 'A') of a scale a few times larger than the convective rolls (which appear everywhere inside the cores as smaller streamwise streaks) are observed in the braid. The amplitude of these streaks, as determined by the sharpness of the lines, tapers away with increasing distance from the localized pairing, indicating that the streaks are intimately tied to the presence of the localized pairing. The scale, behaviour and appearance of these structures are

consistent with our observations of co-rotating streamwise vortices. This observation suggests that a mixing layer does not need a 'global' cross-shear to develop the co-rotating streamwise vortices. A three-dimensional phenomenon such as a localized pairing could generate local cross-shear baroclinically where the local curvature of the density interface contains a large $\partial\rho/\partial z$ component.

4.3. *Mixing measurements*

Figure 26(*a*) illustrates the influence of cross-shear upon the total yield of mixed fluid (mixed-fluid thickness, δ_m). The cross-shear is introduced at about the onset of the main Kelvin–Helmholtz instability. In varying the cross-shear we keep the total energy budget of the mixing layer fixed, by adjusting the strength of the main shear so that the resultant shear is the same in all cases. If the level of cross-shear is low ($< 15\%$), the amount of mixing actually decreases because energy is taken out of the primary shear layer which reduces its mixing capacity, and put into cross-shear which is not yet strong enough to induce co-rotating streamwise vortices. Beyond a critical level of cross-shear, the streamwise instability is able to form, resulting in a sharp increase in mixing. The co-rotating streamwise vortices are aligned along the principle axis of strain in the braid and, therefore, would experience large vortex stretching and generate a considerable amount of turbulent stresses and small-scaled fluctuations. In a simple two-dimensional mixing layer, most of the entrainment and mixing are observed in the primary vortices. The presence of streamwise vortices would add to entrainment and mixing by generating small-scaled fluctuations in the braid. Flow visualization also reveals strong interaction between the streamwise and the primary vortices, possibly increasing the turbulence production and mixing in the primary vortices themselves. Since the streamwise vortices grow through pairings to a size comparable to the primary vortices, the interaction between the two types of structures can be significant, resulting in more mixing and possibly earlier transition.

Figure 26(*b*) illustrates the effect of timing in introducing cross-shear upon the total yield of mixed fluid (keeping the level of cross-shear fixed at 25% of the main shear). It is found that if cross-shear is introduced too early while the shear layer is still planar, the resulting flow behaves simply as a normal but oblique two-dimensional mixing layer. The co-rotating streamwise vortices and the corresponding added mixing result only when cross-shear is introduced after the primary shear layer has started to roll up, the reason being that the streamwise vortex is an instability of the braid and therefore the braid needs to be set up in order for the streamwise instability to develop. If cross-shear is introduced too late, the streamwise vortices might not be able to develop as strongly because the stretching in the braid decreases with time as the stabilizing effect of stratification acts to dissipate the energy of the primary vortices.

5. Discussion

Shear and buoyancy are the two main forces that determine structures and flow dynamics in a turbulent stratified mixing layer. The shear-induced features of the flow, though dominant, are affected in significant ways by the presence of even moderate stratification. Stable stratification has a stabilizing effect on the growth and dynamics of the primary Kelvin–Helmholtz instability, resulting not only in smaller overall fluid entrainment but also an entrainment ratio that is less favourable to efficient mixing. Stratification also reduces pairing interactions among the large-scale vortices, which have for some time been identified with the mixing transition (Winant & Browand 1974; Jimenez 1983). After the turbulent transition, the presence of stratification

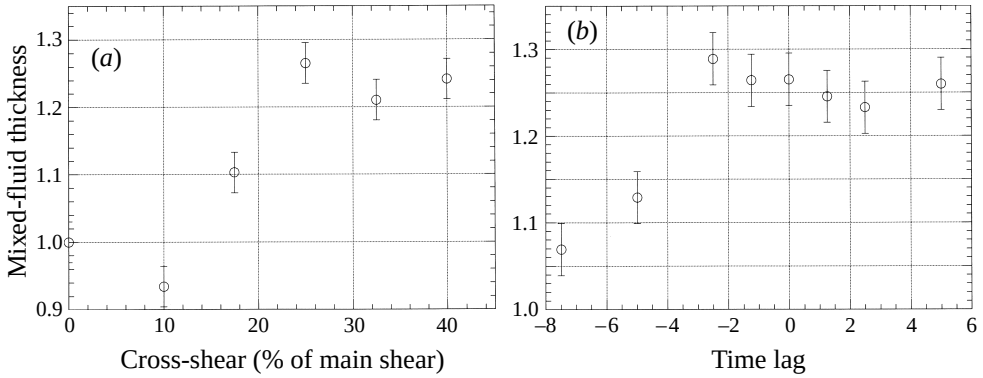

FIGURE 26. (*a*) Plot of final mixed-fluid thickness *vs.* cross-shear strength. The mixed-fluid thickness is normalized so that the value at zero cross-shear is 1. (*b*) Plot of final mixed-fluid thickness *vs.* the point in time when the cross-shear is introduced, for a fixed cross-shear strength of 25% of the main shear. Zero time is when the large-scale Kelvin–Helmholtz instability is first visible. The mixed-fluid thickness is normalized so that the value at zero cross-shear is 1. The time lag is normalized with the overturning time scale $\lambda_{KH}/(\Delta U_m/2)$.

eventually causes the flow to relaminarize and restratify as vertical mixing processes become stabilized.

The main prerequisite to a mixing transition is a large increase in the diffusive interface where the top and bottom fluids are brought into direct contact so they can mix in the molecular sense; this is particularly true in aqueous flows which have a small molecular diffusivity. Meeting this requirement is generally attributed to the onset of small-scale three-dimensional motions through a cascade of secondary two-dimensional and three-dimensional instabilities such as secondary shear-induced instability and convective instability. But even before the onset of small-scale transition, the diffusive interface between the top and bottom fluids can exponentially increase by more than 20-fold by complex kinematics during the first pairing of the Kelvin–Helmholtz vortices. This phenomenon not only directly contributes to the required diffusive interface but also effectively 'stirs' the fluids so that once the small-scale transition takes place the fluids may be mixed more efficiently. Previously, Jimenez & Martel (1991) observed a transition during the first pairing in a numerical two-dimensional mixing layer where the fractal geometry of the material interface increases from a low initial dimension of about 1–1.2 to a higher one of about 5/3. Min (1994) observed exponential line stretching of the interface in a two-dimensional mixing layer after the second pairing, indicating chaotic behaviour.

Although stable stratification has a net effect of reducing the overall mixing, there are two mechanisms associated with buoyancy which actually have quite the reverse effect. A secondary shear-induced instability can develop at locations where the local Richardson number is low enough. This type of instability is usually found in the braid but sometimes occurs on the crests of large-scale vortices. Secondly, the statically unstable regions inside the cores of large-scale vortices can support gravitational convective instabilities. These two secondary instabilities would naturally add to the overall mixing in the mixing layer, but the effect is only secondary compared with the stabilizing effect of stratification.

Shear flows in the natural environment and practical applications are rarely two-dimensional or steady. If the base flow changes in such a way as to introduce a global cross-shear or a local phenomenon such as a localized pairing creates a large enough local cross-shear, co-rotating streamwise vortices may develop. Scenarios in which one

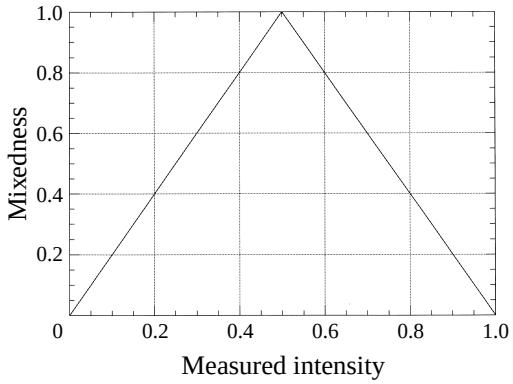

FIGURE 27. Mixedness calculated from the measured fluorescent intensity of each measuring volume.

might encounter cross-shear are stratified mixing layers over three-dimensional topography, wave–mixing layer interaction, and shear flows in complex engineering systems. Although current observations provide some basic understanding, important questions still remain, such as whether co-rotating streamwise vortices can become active on the scales of oceanographic and atmospheric interest, and if so how important they are compared to other mixing events in determining the overall dynamics of the flow and in deriving accurate estimates of flux quantities.

We sincerely thank Professors A. Roshko, C. D. Winant, P. E. Dimotakis, and A. Leonard for the valuable discussions which contributed a great deal to this work. This work was supported by DARPA grant N00014-91-J-1968.

Appendix

The flow parameters such as speed and viscous diffusion length scale can be analytically derived from fundamental equations (see Thorpe 1968 for detailed derivations). From these calculations, flow parameters such as the Reynolds number and the Richardson number can be estimated.

The velocity difference between the two layers can be written as

$$\Delta U = U_t - U_b = \frac{\Delta\rho}{\bar{\rho}} gt \sin\theta.$$

The ratio Q is equal to δ_ρ/δ_v and has the form

$$Q = \frac{2}{1+(1+4\pi\nu t/\delta_\rho^2)^{1/2}}.$$

The flow Reynolds and Richardson numbers are approximately given by

$$Re = \frac{\Delta U \delta_\rho}{\nu Q} = \left(\frac{\Delta\rho}{\bar{\rho}} gt \sin\theta\right)\frac{\delta_\rho}{\nu Q}, \quad Ri = \frac{g\Delta\rho\delta_\rho}{\bar{\rho}(\Delta U)^2 Q^2}.$$

In using these equations to estimate flow parameters at any given time, the time t is measured from a 'virtual' zero time since it is not possible to tilt the tank to the desired angle instantaneously, nor is it desirable to. The virtual zero time is defined to be at the halfway point in the tilting process. For smooth tilting, it takes 3 s to tilt the tank from horizontal to the desired angle; therefore, the virtual zero time is 1.5 s from the initiation of tilt. The calculation of flow velocity in this manner provides a good

estimate to within 3%, as calibrated by measuring the velocity of neutrally buoyant particles in the base flows.

From the density field measured using the LIF method as described in §2.5, we can obtain statistical quantities about the mixed turbulent fluids. A quantity called mixedness, $M(t, y)$ (Konrad 1976) is defined as

$$M(t,y) = \frac{\int_{x_1}^{x_2} H(\rho-\bar{\rho})\,(\rho_b-\rho)\,\mathrm{d}x + \int_{x_1}^{x_2} H(\bar{\rho}-\rho)\,(\rho-\rho_t)\,\mathrm{d}x}{\int_{x_1}^{x_2} H(\rho-\bar{\rho})\,(\rho_b-\bar{\rho})\,\mathrm{d}x + \int_{x_1}^{x_2} H(\bar{\rho}-\rho)\,(\bar{\rho}-\rho_t)\,\mathrm{d}x},$$

where x_1 and x_2 are the edges of the region of interest, and H is the Heaviside step function defined as

$$\begin{aligned} H(f) &= 1 \quad \text{for } f \geqslant 0 \\ &= 0 \quad \text{for } f > 0. \end{aligned}$$

The mixedness is zero when the fluorescent intensity registers 0 or 1, meaning the fluid in the measuring volume consists only of either fluid from the top or from the bottom layer. The mixedness would be 1 if the measuring volume records an intensity of 0.5, meaning that there is an equal amount of top and bottom fluid in the measuring volume and that the measuring volume consists entirely of mixed fluid, provided the spatial resolution of the recording system can resolve the smallest diffusion scale. Figure 27 depicts the mixedness as a function of measured intensity.

And finally the mixed-fluid thickness δ_m is defined as the following:

$$\delta_m(t) = \int_{-h/2}^{h/2} M(t,y)\,\mathrm{d}y$$

where h is the depth of the tank.

REFERENCES

Bernal, L. P. & Roshko, A. 1986 Streamwise vortex structure in plane mixing layers. *J. Fluid Mech.* **170**, 499.

Breidenthal, R. 1978 Chemically reacting, turbulent shear layer. PhD thesis, California Institute of Technology.

Browand, F. K. & Troutt, T. R. 1980 A note on spanwise structure in the two-dimensional mixing layer. *J. Fluid Mech.* **97**, 771.

Brown, G. L. & Roshko, A. 1974 On density effects and large structure in turbulent mixing layers. *J. Fluid Mech.* **64**, 775.

Browning, K. A. & Watkins, C. D. 1970 Observations of clear air turbulence by high power radar. *Nature* **227**, 260.

Chien, W.-L., Rising, H. & Ottino, J. M. 1986 Laminar mixing and chaotic mixing in several cavity flows. *J. Fluid Mech.* **170**, 355.

Corcos, G. M. & Sherman, F. S. 1984 The mixing layer: deterministic models of a turbulent flow. Part 1. Introduction and the two-dimensional flow. *J. Fluid Mech.* **139**, 29.

Dimotakis, P. E. & Brown, G. L. 1976 The mixing layer at high Reynolds number: large-structure dynamics and entrainment. *J. Fluid Mech.* **78**, 535.

Dritschel, D. G., Haynes, P. H., Juckes, M. N. & Shepherd, T. G. 1991 The stability of a two-dimensional vorticity filament under uniform strain. *J. Fluid Mech.* **230**, 647.

Hazel, P. 1972 Numerical studies of the stability of inviscid stratified shear flows. *J. Fluid Mech.* **51**, 39.

Ho, C.-M., Zohar, Y., Foss, J. K. & Buell, J. C. 1991 Phase decorrelation of coherent structures in a free shear layer. *J. Fluid Mech.* **230**, 319.

Jimenez, J. 1983 A spanwise structure in the plane shear layer. *J. Fluid Mech.* **132**, 319.

Jimenez, J. & Martel, C. 1991 Fractal interfaces and product generation in the two-dimensional mixing layer. *Phys. Fluids* A **3**, 5.

Klaassen, G. P. & Peltier, W. R. 1985 The onset of turbulence in finite-amplitude Kelvin–Helmholtz billows. *J. Fluid Mech.* **155**, 1.

Konrad, J. H. 1977 An experimental investigation of mixing in two-dimensional turbulent shear flows with applications to diffusion-limited chemical reactions. PhD thesis, California Institute of Technology.

Koochesfahani, M. M. & Dimotakis, P. E. 1986 Mixing and chemical reactions in a turbulent liquid mixing layer. *J. Fluid Mech.* **170**, 83.

Koop, C. G. & Browand, F. K. 1979 Instability and turbulence in a stratified fluid with shear. *J. Fluid Mech.* **93**, 135.

Lasheras, J. C. & Choi, H. 1988 Three-dimensional instability of a plane free shear layer: an experimental study of the formation and evolution of streamwise vortices. *J. Fluid Mech.* **189**, 53.

Liepmann, H. W. & Laufer, J. 1947 Investigation of free turbulent mixing. *NACA Tech. Note* 1257.

Lin, S. J. & Corcos, G. M. 1984 The mixing layer: deterministic models of a turbulent flow. Part 3. The effect of plane strain on the dynamics of the streamwise vortices. *J. Fluid Mech.* **141**, 139.

McDougall, T. J. 1979 On the elimination of refractive-index variations in turbulent density-stratified liquid flows. *J. Fluid Mech.* **93**, 83.

Min, I. A. 1994 Transport, stirring and mixing in two-dimensional vortex flows. PhD thesis, California Institute of Technology.

Patnaik, P. C., Sherman, F. S. & Corcos, G. M. 1976 A numerical simulation of Kelvin–Helmholtz waves of finite amplitude. *J. Fluid Mech.* **73**, 215.

Pierrehumbert, R. T. & Widnall, S. E. 1982 The two- and three-dimensional instabilities of a spatially periodic shear layer. *J. Fluid Mech.* **114**, 59.

Schowalter, D. G., Van Atta, C. W. & Lasheras, J. C. 1994 A study of streamwise vortex structure in a stratified shear layer. *J. Fluid Mech.* **281**, 247.

Staquet, C. 1995 Two-dimensional secondary instabilities in a strongly stratified shear layer. *J. Fluid Mech.* **296**, 73.

Staquet, C. & Riley, J. J. 1989 A numerical study of a stably-stratified mixing layer. In *Turbulent Shear Flows 6* (ed. J.-C. André *et al.*), pp. 381–397. Springer.

Taylor, G. I. 1950 The instability of liquid surfaces when accelerated in a direction perpendicular to their planes I. *Proc. R. Soc. Lond.* A **201**, 192.

Thorpe, S. A. 1968 A method of producing a shear flow in a stratified fluid. *J. Fluid Mech.* **32**, 693.

Thorpe, S. A. 1971 Experiments on the instability of stratified shear flows: miscible fluids. *J. Fluid Mech.* **46**, 299.

Thorpe, S. A. 1973 Experiments on instability and turbulence in a stratified shear flow. *J. Fluid Mech.* **61**, 731.

Thorpe, S. A. 1985 Laboratory observations of secondary structures in Kelvin–Helmholtz billows and consequences for ocean mixing. *Geophys. Astrophys. Fluid Dyn.* **34**, 175.

Thorpe, S. A. 1987 Transitional phenomena and the development of turbulence in stratified fluids: a review. *J. Geophys. Res.* **92**, 5231.

Thorpe, S. A. & Holt, J. T. 1995 The effects of laterally sloping upper and lower boundaries on waves and instability in stratified shear flows. *J. Fluid Mech.* **61**, 731.

Winant, C. D. & Browand, F. K. 1974 Vortex pairing: the mechanism of turbulent mixing-layer growth at moderate Reynolds number. *J. Fluid Mech.* **63**, 237.

Woods, J. D. 1968 Wave-induced shear instability in the summer thermocline. *J. Fluid Mech.* **32**, 791.